Excitation transfer induced spectral diffusion and the influence of structural spectral diffusion

Daniel E. Rosenfeld and Michael D. Fayer[a)]
Department of Chemistry, Stanford University, Stanford, California 94305, USA

(Received 27 May 2012; accepted 23 July 2012; published online 10 August 2012)

The theory of vibrational excitation transfer, which causes spectral diffusion and is also influenced by structural spectral diffusion, is developed and applied to systems consisting of vibrational chromophores. Excitation transfer induced spectral diffusion is the time-dependent change in vibrational frequency induced by an excitation on an initially excited molecule jumping to other molecules that have different vibrational frequencies within the inhomogeneously broadened vibrational absorption line. The excitation transfer process is modeled as Förster resonant transfer, which depends on the overlap of the homogeneous spectra of the donating and accepting vibrational chromophores. Because the absorption line is inhomogeneously broadened, two molecules in close proximity can have overlaps of their homogeneous lines that range from substantial to very little. In the absence of structural dynamics, the overlap of the homogeneous lines of the donating and accepting vibrational chromophores would be fixed. However, dynamics of the medium that contains the vibrational chromophores, e.g., a liquid solvent or a surrounding protein, produce spectral diffusion. Spectral diffusion causes the position of a molecule's homogeneous line within the inhomogeneous spectrum to change with time. Therefore, the overlap of donating and accepting molecules' homogeneous lines is time dependent, which must be taken into account in the excitation transfer theory. The excitation transfer problem is solved for inhomogeneous lines with fluctuating homogeneous line frequencies. The method allows the simultaneous treatment of both excitation transfer induced spectral diffusion and structural fluctuation induced spectral diffusion. It is found that the excitation transfer process is enhanced by the stochastic fluctuations in frequencies. It is shown how a measurement of spectral diffusion can be separated into the two types of spectral diffusion, which permits the structural spectral diffusion to be determined in the presence of excitation transfer spectral diffusion. Various approximations and computational methodologies are explored. [http://dx.doi.org/10.1063/1.4742762]

I. INTRODUCTION

The transfer of an electronic excitation among molecules in dense media has been studied for over two thirds of a century.[1–4] Using the theoretical framework devised by Förster, electronic excitation transfer has been analyzed in polymer systems,[5–7] micelles,[8] solutions,[9–13] mixed crystals,[14] two-dimensional systems,[15,16] and biological systems.[17–21] Recently, there has been considerable interest in developing a firm theoretical understanding of ultrafast time-dependent *vibrational* spectroscopy of dense media. The systems studied include proteins and other biological molecules,[1,17,20,21] water (and isotopically labeled water),[22,23] clusters of ions in solution,[24,25] phospholipid bilayers,[26] and most recently self-assembled molecular monolayers of catalytically active molecules.[27] In particular, 2D IR vibrational echo spectroscopy is employed to measure spectral diffusion. Spectral diffusion is the time evolution of the vibrational frequencies of molecular vibrational oscillators within an inhomogeneously broadened absorption line.[28–30] The interest in spectral diffusion is that it is caused by structural evolution of the system. Therefore, the time dependence of spectral diffusion reports on the time dependence of structural changes of a system such as a liquid,[30] or a protein.[31]

In addition to structural changes, there can be another source of spectral diffusion. If the vibrational chromophores are close to each other, vibrational excitation transfer (ET) can occur.[32–34] In general, two molecules that are physically near each other will not have the same vibrational frequency because they will have different local environments. When an excitation jumps from an initially excited molecule to a nearby molecule, the frequency of the excitation will change. Therefore, excitation transfer is a source of spectral diffusion. To avoid this source of spectral diffusion in ultrafast IR studies of water dynamics, the OD stretch of dilute HOD in H_2O is studied.[35] Because the HODs are dilute, excitation transfer is eliminated. In pure H_2O, excitation transfer in itself is of interest, and it dominates spectral diffusion.[23,36] However, in other systems excitation transfer cannot be avoided,[27] but the source of spectral diffusion that is of interest is the structural spectral diffusion (SSD). Therefore, it is necessary to be able to accurately calculate the excitation transfer induced spectral diffusion so that it can be separated from the structural spectral diffusion. As shown in detail here, the problem is complex because the structural spectral diffusion has a strong influence on the excitation transfer induced spectral diffusion.

a)fayer@stanford.edu.

In addition, the Förster theory of excitation transfer requires knowledge of the overlap of the *homogeneous spectra* of the donating and accepting molecules.[4,37,38] For electronic excitations, it is assumed that the spectroscopic lines are homogeneously broadened (no inhomogeneous broadening). Electronic excitations generally have a large Stokes shift between the absorption and fluorescence spectra. The necessary overlap is the overlap of the absorption and fluorescence spectra.[4,37] Vibrational absorption lines usually have substantial inhomogeneous broadening. The homogeneous spectra of the donor and acceptor are buried under the inhomogeneous lines. (Here we use donor to be the initially excited molecule and acceptor to be the molecule that receives the excitation although the two molecules are chemically identical.) Therefore, it is necessary to perform a 2D IR vibrational echo experiment to determine the homogeneous linewidth,[39,40] which is a necessary input for the Förster theory and the theoretical method developed below.

A preliminary version of the theory, which is developed fully here, was used to interpret 2D IR vibrational echo spectroscopic data for samples that consisted of approximately a monolayer of molecules bound to a surface.[27] In these systems, the proximity of chromophores indicated that excitation transfer plays a significant role in determining the observed vibrational spectral diffusion, and therefore excitation transfer needed to be treated properly to obtain the underlying molecular structural dynamics. As mentioned above, in vibrational systems, spectral lines are inhomogeneously broadened, which precludes the use of standard Förster type results, which depend on the underlying transitions being homogeneously broadened. Not only are the spectral lines in vibrational systems inhomogeneous, they also undergo spectral diffusion that can be on the same timescale as excitation transfer. A simultaneous solution to the coupled excitation transfer and structural spectral diffusion processes is necessary. This paper presents several useful calculations for these systems: (1) excitation transfer in the case of static inhomogeneous lines (no structural spectral diffusion), (2) spectral diffusion induced by excitation transfer, and (3) spectral diffusion in the case of excitation transfer and structural spectral diffusion processes.

Despite the keen interest in developing an understanding of the vibrational spectral dynamics in the condensed phases, there has not been an acceptable framework developed for understanding how excitation transfer occurs in these systems. In fact, researchers have applied Förster theory in situations in which the theory is not applicable. Although Förster theory has been exceptionally powerful in understanding excitation transfer among homogeneously broadened electronically excited molecules, many of the simplifying assumptions that apply well to electronic spectroscopy simply do not hold when vibrations are considered. The primary assumption that fails for most vibrational systems is the assumption that all spectral lines are purely homogeneously broadened. This complication was observed for the case of electronic transitions nearly 40 yr ago in the Russian literature,[41–43] but these observations have been considered seriously only in the case of the electronic excited state dynamics of photosynthetic complexes[44–47] and dispersive excitation transport in liquids and polymers.[7,9,48] The work of Stein and Fayer incorporates spectral diffusion into a theory of dispersive excitation transport, yet the theory only applies to the case of narrowband excitation experiments (such as hole burning, fluorescence) and is difficult to generalize. Stein and Fayer do not examine the general aspects of excitation transfer induced spectral diffusion (ETISD), its coupling to SSD, or computational methodologies that allow for the calculation of an observable other than the self part of the excitation transfer Green's function.[9]

Förster theory describes the transfer of excitation between two chromophores through dipole-dipole coupling.[4] The transfer rate can be calculated either by Fermi's golden rule or second-order time-dependent perturbation theory in the density matrix formalism.[23,49,50] The Förster limit corresponds to weak incoherent transfer. When the coupling is sufficiently strong or the transfer is coherent, Förster theory does not apply, and a fully quantum mechanical treatment is necessary to solve the excitation transfer problem.[51] If the excitation transfer problem is in the Förster limit, then a master equation formalism can be used to calculate the effects of excitation transfer on the excitation probabilities in a system.[47] This paper focuses on results derived from the master equation approach, although despite this limitation, that the general ideas should shed some light on strongly coupled systems.

Structural spectral diffusion is the stochastic fluctuation among inhomogeneous spectral states.[28,30] The process can be characterized by its correlation functions. If the fluctuations are Gaussian (or reasonably approximated as Gaussian), then the process is fully characterized by its autocorrelation function that is called the frequency-frequency correlation function (FFCF). If the FFCF is known, then the absorption and 2D IR spectroscopic line shapes can be calculated, linking the observed spectroscopy to the microscopic dynamics. Furthermore, in the higher order nonlinear optical experiments, that is, 2D IR vibrational echoes, the FFCF can be directly measured.[39,52] The FFCF includes both the spectral diffusion among the inhomogeneous states and the homogeneous linewidth.

Within an inhomogeneous line, transfer of an excitation from an excited chromophore to a different chromophore with a different frequency will also contribute to the decay of the FFCF. Calculating the full FFCF requires taking into account both structural processes and the excitation transfer process itself. These processes together form a coupled stochastic nonlinear dynamic system, the practical solution of which is the major goal of this paper.

Recently, other researchers have studied spectral diffusion in systems undergoing excitation transfer. Yang, Li, and Skinner recently published an analysis of energy transport in liquid H_2O, D_2O, and isotopically diluted mixtures.[22,23] Their analysis is based upon a solution of the time-dependent Schrodinger equation for the manifold of local vibrational states using molecular dynamics (MD) trajectories to define the atomic coordinates. Their theory satisfactorily agrees with experimental measurements of the orientational anisotropy decay.[23] Due to the nearly first principles approach, Skinner and co-workers have validated that perturbation theory adequately describes excitation transfer even in extremely strongly coupled situations (like liquid water) and that the

majority of the transfer is incoherent.[23] Despite the fact that the system is in the Förster limit, a naïve application fails to agree with experiments that probe the underlying excitation transfer process. Skinner and co-workers say that by including orientational effects, a proper radial distribution function, and intramolecular excitation transfer, Förster theory can be made to agree with experimental anisotropy data. However, Skinner and co-workers have illuminated the pitfalls of applying Förster theory to vibrational energy transport. Their extension of Förster theory utilizes only a single Förster radius, R_0, which in principle cannot account for vibrational excitation transport between different types of pairs of water molecules, i.e., for randomly chosen pairs of water molecules, not only do their relative orientations and distances differ but also the center frequencies of their homogeneous lines will differ. Because R_0 depends on the overlap of the homogeneous lines, different pairs of molecules will have different R_0's. While Skinner's *ab initio* theory correctly incorporates frequency fluctuations and frequency differences among pairs of exchanging water molecules, no attempt was made to correctly incorporate this fundamental aspect of the excitation transfer process into a modified Förster theory. However, the nature of water may mask this inadequacy. The homogeneous linewidth in water is very broad; it is a substantial fraction of the total linewidth. In addition, much of the structural spectral diffusion is very fast, occurring on the order of a few hundred femtoseconds. These properties of the water hydroxyl stretch spectral dynamics are in many respects similar to those found in electronic excitation transfer systems consisting of chromophores in room temperature liquids in which the simple Förster theory generally works well. Water is unique in this respect. Many vibrations have homogeneous lines that are much narrower than the inhomogeneous linewidth and have relatively slow structural spectral diffusion. In these systems, simple Förster theory with a single R_0 will not provide a useful description of the vibrational excitation transfer and its contribution to spectral diffusion.

II. EXCITATION TRANSFER INDUCED SPECTRAL DIFFUSION IN THE STATIC FREQUENCY LIMIT

The failure of nearly every attempt to use Förster theory to explain vibrational excitation transfer can be reduced to the fact that the expectation value of a function of a random variable is not equal to the function evaluated at the expectation value of the random variable, i.e., $\mathrm{E}[f(x)] \neq f(\mathrm{E}[x])$. In certain special cases ($f(x)$ is linear, x is deterministic), the equality can hold, but none of these cases applies to vibrational ET. In the language of ET theory, x is the transfer rate between two randomly selected molecules and $f(x)$ is an experimental observable. $f(x)$ could be the frequency-frequency correlation function, the anisotropy decay, or simply the amount of population left on the initially excited molecule. For the case of the frequency-frequency correlation function, the desired expectation value is

$$\begin{aligned}\langle \delta\omega(t)\delta\omega(0)\rangle &= \mathrm{E}_{\{\mathbf{r},\omega\}}[f(\mathbf{r},\omega;t)] \\ &= \mathrm{E}_{\{\mathbf{r},\omega\}}\left[\mathrm{E}\left[\delta\omega(t)\delta\omega(0)|\{\mathbf{r},\omega\}\right]\right], \end{aligned} \quad (1)$$

where $\langle \delta\omega(t)\delta\omega(0)\rangle$ is the frequency-frequency correlation function which depends on the position related variables of the system $\mathbf{r}$, and the frequency related variables of the system ω.

In this paper we explicate Förster theory in the inhomogeneous case and demonstrate how the excitation transfer process can drive not only spectral diffusion but also be driven by structural spectral diffusion. The initial inhomogeneous Förster theory is modified to account for structural spectral diffusion, and tractable approximations are made that greatly simplify the calculations. Due to recent work on surface systems undergoing spectral diffusion and ET simultaneously, extra attention is given to the two-dimensional case.[27]

A. Excitation transfer for an ensemble of particle pairs

In the case when vibrations do not undergo structural spectral diffusion, there is only homogeneous and inhomogeneous spectral line broadening. When two spatially proximate molecules are chosen at random from the inhomogeneous distribution of vibrational frequencies, they may undergo ET. Because these molecules belong to different sub-ensembles and are not coupled by any mechanism other than dipole-dipole coupling (which is assumed to be relatively weak and incoherent), the classical Förster theory applies.[4] Within this theory, the rate of ET depends on the difference in center frequencies and the homogeneous linewidths. We can calculate the probability of the excitation moving between these two molecules. For two molecules undergoing reversible ET, the coupled differential equations which describe the ET process are written as

$$\begin{aligned}\dot{p}_0 &= -kp_0 + kp_1, \\ \dot{p}_1 &= +kp_0 - kp_1, \end{aligned} \quad (2)$$

where k is the Förster transfer rate, p_0 denotes the probability of the excitation residing on the initially excited molecule, and p_1 is the probability of excitation residing on the non-initially excited molecule. Vibrational population relaxation has been omitted as it is assumed to be the same for all molecules and therefore can be added in later as decay in the overall probability of finding the excitation anywhere. The solution to these coupled differential equations for the initial condition $p_0 = 1$; $p_1 = 0$ is $p_0(t) = \frac{1}{2}(1 + e^{-2kt})$. This probability is also denoted as the self part of the Green's function, $G_s(t)$, which comes into play when there are more than two chromophores. The rate k is determined by the standard Förster method,[4,38] i.e.,

$$k = \frac{3}{2T_{VR}}\kappa^2(\Omega)\left(\frac{R_0}{r}\right)^6, \quad (3)$$

$$R_0^6 = \frac{9(\ln 10)\kappa^2 Q_D}{128\pi^5 N_A n^4}\frac{\int_0^{+\infty}\lambda^4\varepsilon_A(\lambda)\varepsilon_D(\lambda)d\lambda}{\int_0^{+\infty}\varepsilon_D(\lambda)d\lambda}, \quad (4)$$

where R_0 is the Förster radius, T_{VR} is the vibrational lifetime, Q_D is the quantum yield, N_A is Avogadro's constant, n is the index of refraction of the medium, λ is the wavelength in nm, ε is the molar decadic extinction coefficient (in L mol^{-1} cm^{-1}) and $\kappa^2(\Omega)$ is the dipole-dipole coupling

orientation factor. The quantum yield is the fraction of chromophore excitations that decay by spontaneous emission, and can be calculated from the radiative lifetime and the nonradiative lifetime. R_0 depends on the frequency distribution of both oscillators and their transition strengths. In Förster theory, the overlap integral that is used to determine R_0 includes the emission line of the donor and the absorption line of the acceptor. In the case of vibrations there is no appreciable Stokes shift, so for a given vibrational oscillator the absorption and emission line position and shape are considered to be the same throughout this paper.

The solutions to the ET problem for two molecules in two different cases (using the parameters from the Appendix) are illustrated in Figure 1. In the first case, the two molecules chosen have vibrations with their homogeneous lines close in frequency (Figure 1(a), blue curves). The overlap between the two absorption lines is large. Therefore, R_0 is large, which makes the transfer rate, k, large. The probability p_0 therefore decays quickly (Figure 1(b), blue curve). In the second case, the molecules are chosen such that their vibrations do not lie close in frequency (Figure 1(a), red curves). In this case the overlap between the two absorption lines is small. So R_0 is small, which makes the transfer rate small. The probability that the excitation resides on the initially excited molecule decays slowly as shown in Figure 1(b) (red curve).

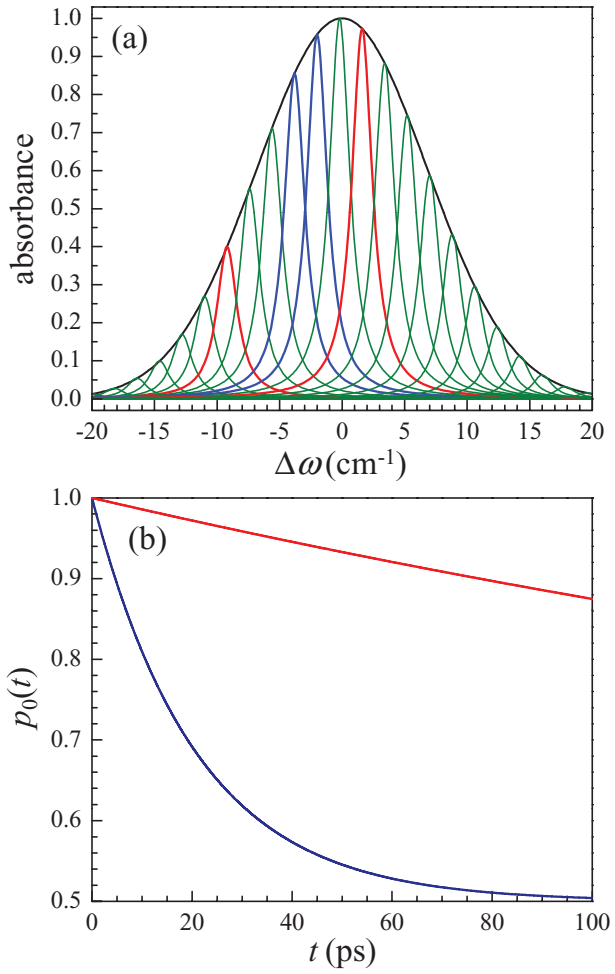

FIG. 1. (a) The inhomogeneous distribution (black curve) of homogeneously broadened vibrational lines (green, red, and blue curves) plotted about the line center. (b) The probability that an initially excited molecule remains excited after a time t in two cases: (red) the exchanging molecules have center frequencies denoted by the red lines in panel (a), (blue) the exchanging molecules have center frequencies denoted by the blue lines in panel (a).

In addition to calculating the probability of ET, our goal here is to also determine the frequency-frequency correlation function of the system undergoing ET. As a simple example consider a system composed of an ensemble of pairs of molecules. In each pair, the two molecules interact with each other but not with other molecules. We can calculate the frequency-frequency correlation function as we know the time-dependent probability distribution of the vibrational frequency. In terms of expectation values, we can calculate the inner expectation of the dynamical observable $\delta\omega(t)\delta\omega(0)|\omega,r$. r was given by the setup of the problem (Appendix), i.e., 8 Å with $\kappa^2 = 2/3$, and the frequencies, which are static at this point, were drawn from the inhomogeneous distribution. In this simple case there are only two probabilities which must be accounted for, the probability that the excitation lies on the initially excited molecule and the probability that it does not. Therefore, the FFCF expectation value is given by the formula

$$\langle \delta\omega(t)\delta\omega(0)\rangle = \mathrm{E}_{\{\delta\omega_1,\delta\omega_2\}}\left[\frac{1}{2}(1+e^{-2k(\omega_1,\omega_2)t})\delta\omega_1^2 + \frac{1}{2}(1-e^{-2k(\omega_1,\omega_2)t})\delta\omega_1\delta\omega_2\right], \quad (5)$$

where $\delta\omega_1$ is the frequency of the initially excited vibration and $\delta\omega_2$ is the frequency of the vibration on the other molecule. The expectation value is the average over the inhomogeneous distribution of frequencies for each vibration. Note that k is a function of $\delta\omega_1$ and $\delta\omega_2$ and therefore must be calculated inside the expectation value. The above solution for the frequency-frequency correlation function is only for spectral diffusion caused by ET. There is no structural spectral diffusion. The homogeneous contribution to the total vibrational line shape can be included by an additional delta function component in the FFCF.[39]

Even in this simple system several key properties of ET are clearly visible. To illustrate them we show the results of ETISD calculation for the ensemble of pairs of molecules. For this calculation we use the numerical inputs chosen for all calculations (see the Appendix). Figure 2 shows the normalized FFCF with the homogeneous component omitted (black curve), the self part of the Green's function (blue curve), and the self part of the Green's function with the Förster radius calculated taking the total spectroscopic line to be homogeneously broadened (red curve), and therefore having unit overlap, instead of using the underlying inhomogeneous distribution of homogeneous line shapes. None of the functions are identical. This figure clearly demonstrates that it is imperative that one performs a detailed ET calculation using the true homogeneous and inhomogeneous line shapes even when calculating the effect of ET on observables uncorrelated with frequency. Using the Förster radius calculated using the entire absorption line yields an incorrect $G_s(t)$ curve that is much too fast. The ETISD itself evolves differently than the ET process

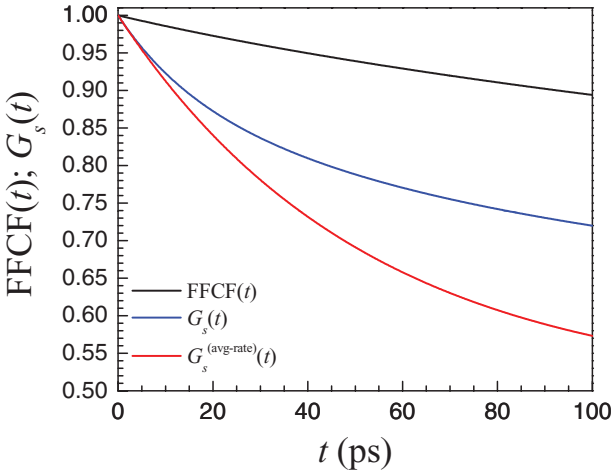

FIG. 2. Normalized FFCF with the homogeneous component omitted for excitation transfer in an ensemble of pairs of particle system (black line). Self part of the Green's function is shown for system studied (blue line) and for a hypothetical purely homogeneously broadened system with the pre-spectrally averaged rate constant (red line).

that drives it, namely, slower. The FFCF decays more slowly than the underlying ET, given as $G_s(t)$ (Figure 2, blue curve) because there is a tradeoff between fast ET and a large frequency change. When molecules are far apart in frequency, there is a large change in frequency when ET occurs. However, the molecules undergo slow ET because the overlap of the homogeneous lines is small. When molecules are close in frequency, they exchange excitations quickly, but the associated change in frequency is small.

Improperly pre-averaging the Förster radius before calculation of ensemble averaged properties is a serious flaw in the manner that Förster theory is frequently used. Förster theory depends on the application of the steady-state approximation to the second-order perturbation theory rate of dipole-dipole coupling induced excitation transfer.[49,50] This approximate rate is itself an ensemble averaged quantity. By ensemble averaging over the entire inhomogeneous distribution in the steady-state approximation step, it becomes impossible to then use the pre-averaged rate to calculate other dynamical observables that must themselves be integrated over the ensemble degrees of freedom. In other words, one cannot use an average rate constant to calculate a kinetic process between distinct sub-ensembles that do not react at the average rate.

The condition that the full underlying homogeneous/inhomogeneous distribution of frequencies needs to be accounted for in an ET problem can be relaxed when the homogeneous linewidth dominates the total absorption line shape. In Figure 3, the same ensemble of pairs of molecules problem is studied but instead of having the homogeneous linewidth, $\Gamma = 2$ cm^{-1} and the inhomogeneous linewidth equal to 16 cm^{-1} (for a total linewidth of 17.1 cm^{-1}) as in Figure 2, Γ is varied from 2 cm^{-1} to 17 cm^{-1}, and the inhomogeneous linewidth is set between 17.1 cm^{-1} and 1.2 cm^{-1} to achieve a total linewidth of 17.1 cm^{-1} for all values of the homogeneous linewidth. The black curves are the normalized FFCF with the homogeneous component omitted. Thus, only the time-dependent part of the FFCF is shown. It is important to keep in mind that as Γ is increased, the range of spectral diffusion is decreased because the inhomogeneous width is decreased. The blue curves are the properly averaged $G_s(t)$, and the red curves are $G_s^{(\text{avg-rate})}(t)$ in which the donor and acceptor are taken to have perfect overlap as if the lines are homogeneously broadened. Several key trends are clear from the figure. First, as the homogeneous linewidth begins to dominate as a fraction of the total linewidth, the time dependence of the frequency-frequency correlation function, and the self part of the Green's function converge. Furthermore, the improperly pre-averaged Förster radius $G_s^{(\text{avg-rate})}(t)$ curve also converges to the true one, indicating that in predominantly homogeneously broadened lines the traditional calculation of the Förster radius (ignoring inhomogeneous line shapes) is accurate. This is the reason that the simplified Förster theory works for water in which the homogeneous linewidth is a substantial fraction of the total linewidth.[23] Also note that as long as there is non-negligible inhomogeneous broadening, ETISD does not track the ET process itself. In Figure 3, only for $\Gamma = 17$ cm^{-1} are the time dependences of ET and ETISD the same, and in this case the range of spectral diffusion is very small. The spectral diffusion induced by ET in an inhomogeneously broadened system can *never* be described by the time dependence of the ET process, no matter how well it is calculated. The homogeneous linewidth must be measured and the

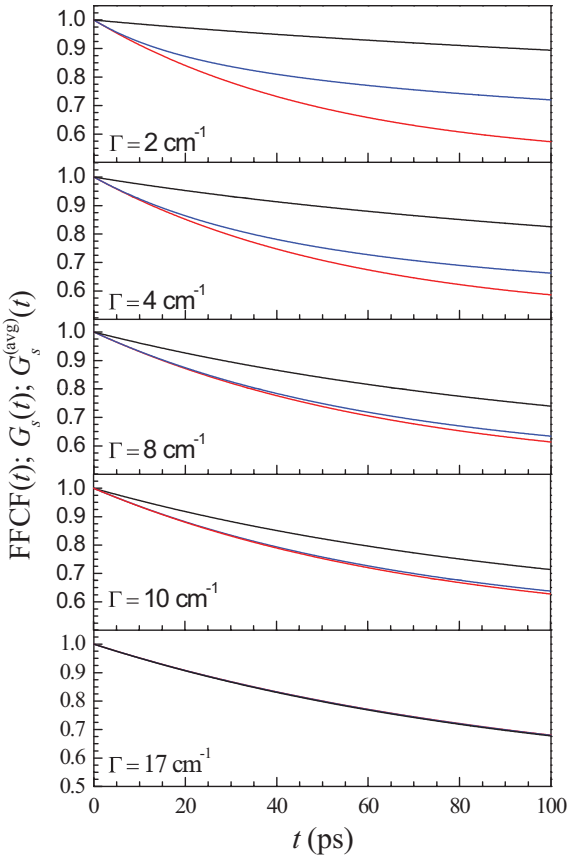

FIG. 3. Normalized FFCF with the homogeneous component omitted (black curve) and self part of the Green's function (actual, blue curve; pre-averaged, red curve), for an ensemble of pairs of particle excitation transfer systems as a function of homogeneous linewidth. The total linewidth is held constant.

inhomogeneous distribution accounted for in calculating the time dependence of the ETISD.

These simple cases encompass the entirety of the physics of vibrational ET theory within the Förster limit. The rest of the work is to build tools to solve this problem efficiently for physically realistic systems rather than an ensemble of isolated pairs. For the remainder of this section we will work within the static frequency limit (no structural spectral diffusion). Once the methodology has been developed we will move on to include stochastically fluctuating structural spectral diffusion.

B. N-particle excitation transfer dynamical system

The two molecule problem can be extended to include N molecules by creating an N-dimensional linear dynamical system (or a master equation; the matrix method is used here for ease of computation) which represents the N coupled linear ordinary differential equations:

$$\dot{\mathrm{p}} = \mathbf{A}(\omega, \mathbf{r})\mathbf{p}, \tag{6}$$

where the vector $\mathbf{p}$ is the vector of probabilities of an excitation being found on a given molecule. The matrix $\mathbf{A}$ is the dynamics matrix and is filled with the rates k_{ij} that are all calculated by the Förster method. The above equation holds for a given set of positions and frequencies. The solution to this problem (with static frequencies and positions) for any initial condition may be given by matrix exponentiation of the dynamics matrix, $\mathbf{A}$,

$$\dot{\mathrm{p}}(t) = \exp\left[t\mathbf{A}\right] \cdot \mathbf{p}(0), \tag{7}$$

where $\mathbf{p}(0)$ is the vector of initial probabilities and $\mathbf{p}(t)$ is the time-dependent probability of finding an excitation on any given molecule. For systems with large N, it becomes intractable to solve this problem analytically; however, for periodic or quasi-periodic systems (such as crystals, liquids, solids, surfaces) periodic boundary conditions can be enforced, for example, by the minimum image criterion, on the dynamics matrix. As long as N is large enough, the results for the periodic systems will be asymptotically equivalent to the results for the bulk system of infinite extent.

Once the time-dependent vector of probabilities is known, then it is possible to calculate the frequency-frequency correlation function for this system. For the case where only a single molecule begins in the excited state, the $\mathbf{p}(0)$ vector is a vector containing a single non-zero element that is equal to 1, that is, $p(0)^{(j\neq i)} = 0$; $p(0)^{(i)} = 1$. Given that the initial excitation begins on the ith molecule, the FFCF for a molecular system with static frequencies given by the inhomogeneous distribution when the frequencies are not correlated with spatial position is

$$\mathrm{E}\left[\omega(t)\omega(0)|\omega,\mathbf{r}\right] = \mathrm{E}\left[\omega(t)\omega(0)|\mathrm{A}(\omega,\mathbf{r})\right] = \left(\mathbf{p}(t)\cdot\boldsymbol{\omega}_t\right)\omega_{t=0}{}^{(i)}. \tag{8}$$

The superscript (i) denotes the ith element of a vector, and the vector $\boldsymbol{\omega}$ contains the center frequency values for each molecule. Note that in the case of time-dependent frequencies (structural spectral diffusion) discussed below, the frequency vectors need not be the same. Also note the clear difference between how the FFCF is calculated versus how $G_s(t)$ is calculated for this system, $G_s(t) = p^{(i)}(t)$.

C. Monte-Carlo based computation of the FFCF

The above solution to the ET induced spectral diffusion problem is based upon a single realization of the static random frequency distribution and a single static realization of the geometric distribution of molecules. To calculate the expectation value of the frequency-frequency correlation function over each of these distributions it is suitable to perform Monte-Carlo averaging. Subsequently, a procedure that simplifies the calculations will be introduced. Thus, returning to the conditional expectation notation, the expected frequency-frequency correlation function is,

$$\begin{aligned}\langle\delta\omega(t)\delta\omega(0)\rangle &= \mathrm{E}_{\{\mathbf{r},\omega\}}\left[\mathrm{E}\left[\delta\omega(t)\delta\omega(0)|\mathbf{A}(\mathbf{r},\omega)\right]\right] \\ &\xrightarrow{\mathrm{MC}} \frac{1}{N}\sum_{\{\omega,\mathbf{r},i\}}\left(\mathbf{p}(t)\cdot\boldsymbol{\omega}\right)\omega^{(i)} = \frac{1}{N}\sum_{\{\omega,\mathbf{r}\}}\sum_{i}\left(\mathbf{p}(t)\cdot\boldsymbol{\omega}\right)\omega^{(i)}.\end{aligned} \tag{9}$$

The outer expectation is over the joint space-frequency distribution function, and the Monte-Carlo summation is a sum over the randomly drawn space-frequency realizations and a randomly chosen initial excitation vector.

For the examples simulated in this paper, the Monte-Carlo averaging is not computational intensive, as spatial distribution functions without higher order structure are chosen. For simulations of real molecular systems, more averaging will be required and Metropolis Monte-Carlo or another Markov Chain Monte-Carlo method will be necessary. For example, we use a uniform random distribution. By drawing independent samples from the uniform random distribution, under 1% error at 95% confidence in the MC estimates can be achieved in under 10^5 samples. When random frequency trajectories are sampled later in the paper, again only simple (i.e., random sampling) Monte-Carlo averaging is necessary, as the higher order structure in the frequency trajectory is generated through the integrated stochastic law we derive for the random process. The sampling is even more efficient when one takes advantage of the fact that multiple initial excitation sites are possible.

III. ETISD AS A PROBE OF STRUCTURE

Due to the r^{-6} dependence of the Förster transfer rate, ET and ETISD are extremely sensitive to the joint space-frequency distribution function of molecules. For the case when frequencies and spatial distribution are independent, and for a given frequency distribution, the excitation transfer and associated ETISD problem are sensitive to the geometric distribution of molecules. This sensitivity can exist in both the distribution of intermolecular distances (through the r^{-6} dependence) and the distribution of relative molecular orientations (through the κ^2 factor). Below we show some general properties of this sensitivity for 1D, 2D, and 3D dimensionalities and implement the Monte-Carlo solution

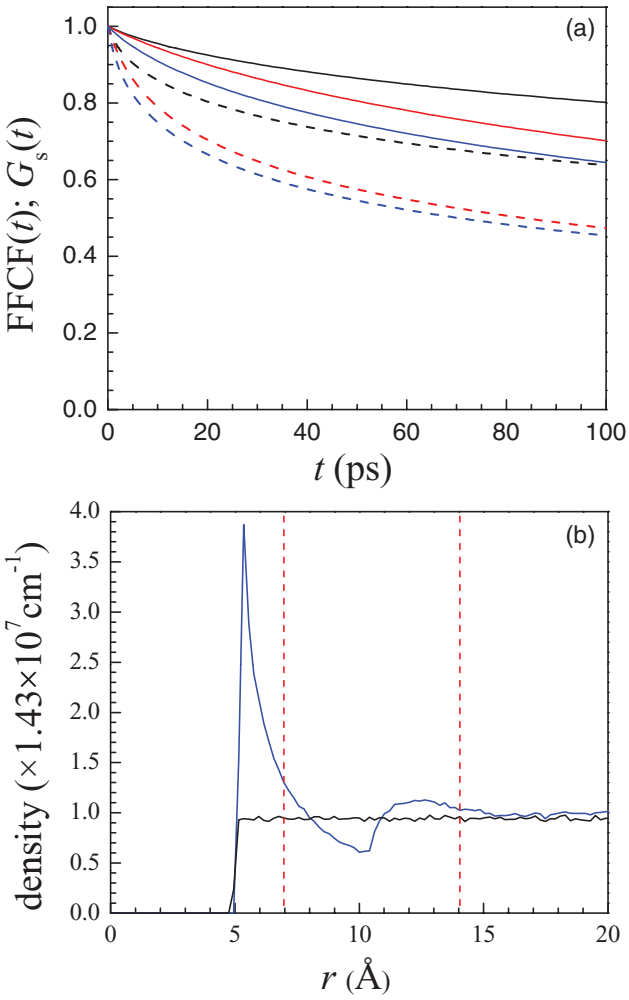

FIG. 4. One-dimensional systems. (a) Normalized FFCFs with the homogeneous component omitted (solid curves) and $G_s(t)$ curves (dashed curves) for random distribution with excluded volume (black), one-dimensional lattice (red line), and hard sphere model (blue line). (b) Radial distribution functions for the corresponding geometric models (same colors) in panel (a). The dashed lines correspond to the lattice sites for the one-dimensional lattice model.

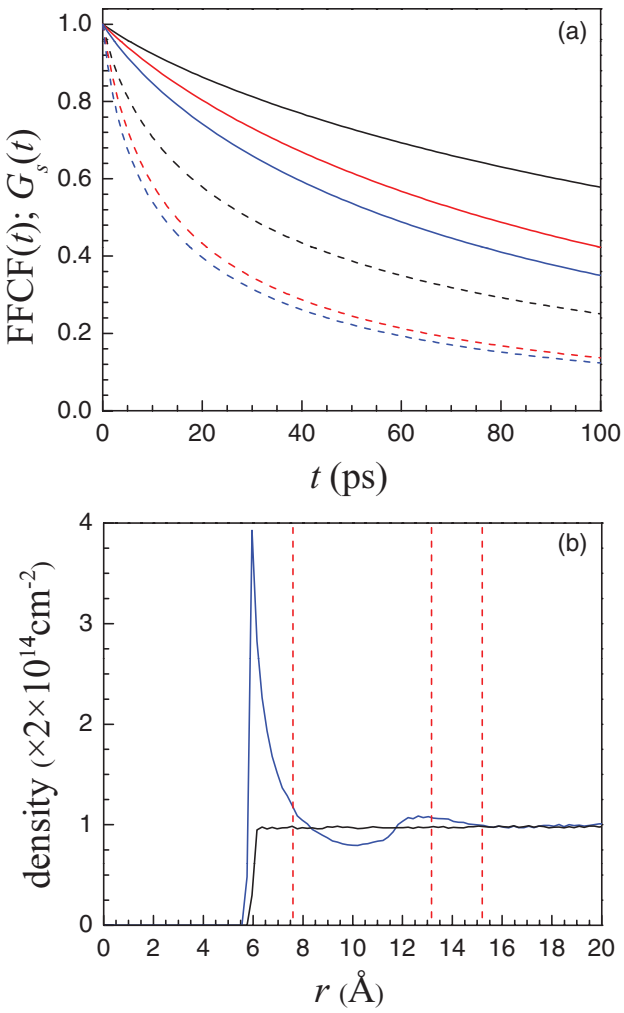

FIG. 5. Two-dimensional systems. (a) Normalized FFCFs with the homogeneous component omitted (solid curves) and $G_s(t)$ curves (dashed curves) for random distribution with excluded volume (black), two-dimensional hexagonal close packed lattice (red line), and hard sphere model (blue line). (b) Radial distribution functions for the corresponding geometric models (same colors) in panel (a). The dashed lines correspond to the lattice sites for the two-dimensional hexagonal lattice model.

to the ETISD problem discussed above. Except for the calculations in Figure 6, the angular factors are static and isotropic, that is, there is a random distribution of fixed orientations.

ETISD is sensitive to the dimensionality of the system. Within a given dimensionality different structures are easily discernible due to their different ETISD profiles. For each dimensionality, three different structures are simulated, a lattice, a loosely packed hard sphere model, and a random distribution with an excluded volume effect. The average density is the same for the three structures. In the 1D systems, the lattice is a linear lattice; in 2D systems it a hexagonal lattice; and in 3D systems it is a simple cubic lattice. The structures differ in their associated radial distribution functions which are visualized in Figures 4(b), 5(b), and 7(b). The different radial densities cause ETISD to proceed at different rates. All calculations use the Monte-Carlo formalism developed above. The Monte-Carlo averaging is performed over both the spatial and frequency dimensions.

Figure 4(a) illustrates the normalized FFCFs with the homogeneous component omitted (solid curves) and $G_s(t)$ (dashed curves) for the three model one-dimensional systems. The black curves are for the random distribution with excluded volume. The red curves are for the 1D lattice, and the blue curves are for the hard sphere model. The radial distribution functions of the three model systems are shown in panel (b) of Figure 4. The dashed lines show the position on the lattice as the distance is increased from the donor molecule. The FFCFs are normalized and the homogeneous contribution is not shown. Parameters for the simulations are given in the Appendix. The random distribution with excluded volume effect is the slowest ETISD system, followed by the linear lattice, followed by the hard sphere model. The differences in ETISD rate are clearly correlated with the radial distribution functions. Specifically, higher local density near an excited molecule drives ETISD due to the strong r^{-6} dependence of the transfer rate.

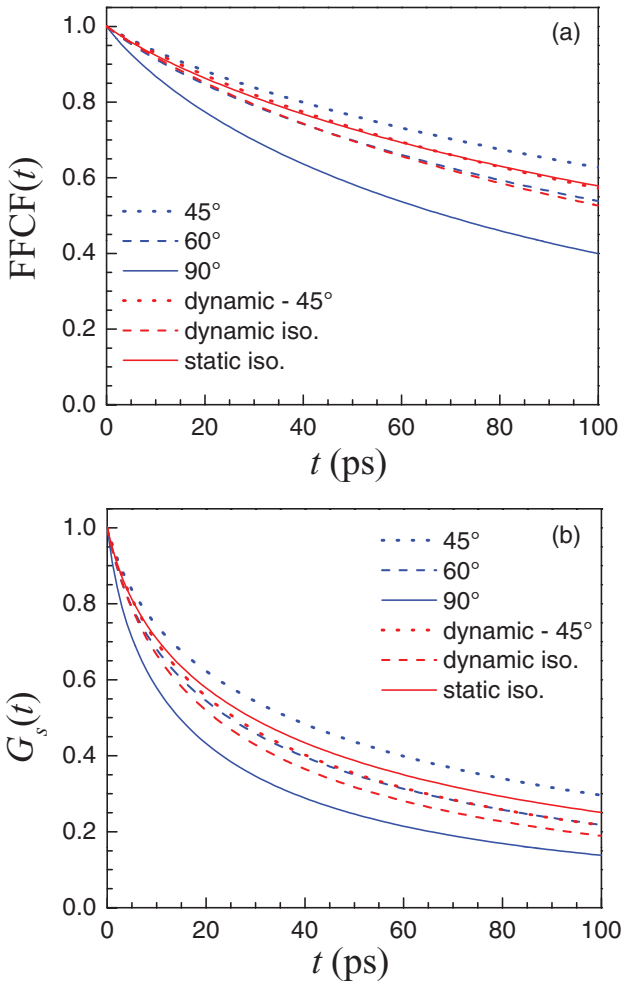

FIG. 6. Two-dimensional systems. (a) Normalized FFCFs with the homogeneous component omitted for six different angular distributions. Blue curves correspond to fixed polar angle models of 45° (dotted), 60° (dashed), and 90° (solid) with respect to the surface normal. Red lines correspond to static isotropic model (solid), dynamic isotropic (dashed), and dynamic with a fixed polar angle of 45° (dotted). (b) $G_s(t)$ curves for the same systems, line designations are the same as in the panel (a).

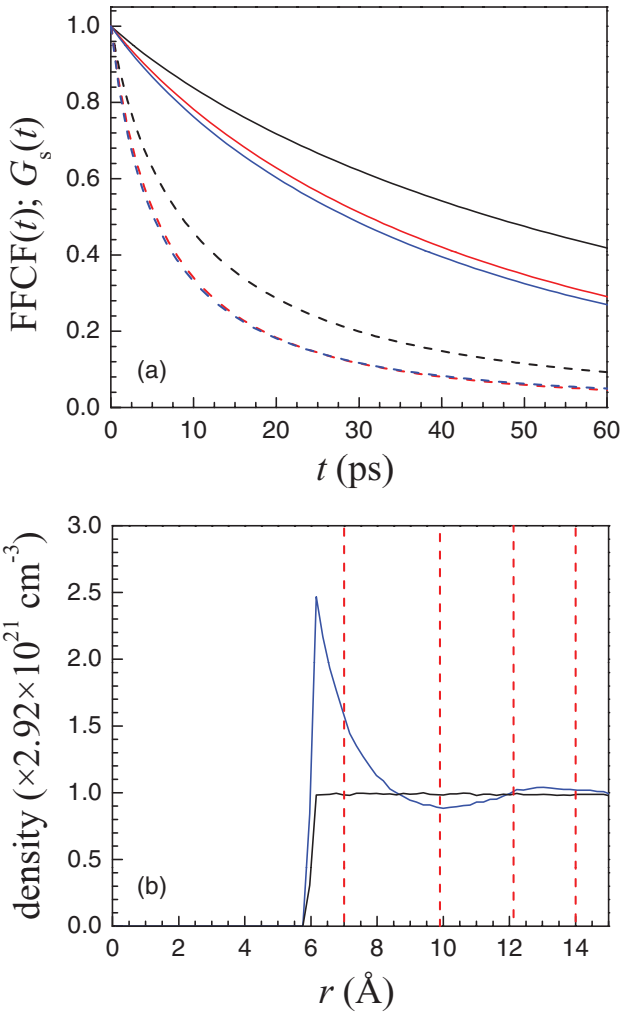

FIG. 7. Three-dimensional systems. (a) Normalized FFCFs with the homogeneous component omitted (solid curves) and $G_s(t)$ curves (dashed curves) for random distribution with excluded volume (black), three-dimensional simple cubic lattice (red), and hard sphere model (blue). (b) Radial distribution functions for the corresponding geometric models (same colors) in panel (a). The dashed lines correspond to the lattice sites for the simple cubic lattice model.

Figure 5(a) illustrates the normalized FFCFs with the homogeneous component omitted (solid curves), and $G_s(t)$ (dashed curves) for the three two-dimensional model systems (monolayers). The hard sphere model has the fastest $G_s(t)$ and ETISD (dashed blue and solid blue curves) due to large peak in the radial distribution function at 5.8 Å (panel b). This increased local density is nearly four times the average density of molecules in the system and serves to enhance ET and ETISD for the hard sphere system. Because the densities are the same, the hexagonal lattice system (red curves) has slower transfer, despite its more efficient packing due to the increased distance between nearest neighbors relative to the hard sphere model. The random distribution with excluded area has the slowest transfer of the three models due to its flat radial distribution function.

The angular distribution for the orientation of the transition dipoles can substantially change the properties of the ETISD and ET process. This effect is illustrated for the two-dimensional system for which several different angular distribution models were analyzed for the random with excluded volume effect model (see Figure 6). The static isotropic model means the transition dipoles are distributed randomly and uniformly in both polar and azimuthal angle. The dynamic isotropic model corresponds to each transition dipole sampling all of angular space on a much faster timescale than excitation transfer. The fixed polar angle model has each chromophore with its transition dipole at an angle θ with respect to the surface normal and is free to lie at any azimuthal angle. The dynamic fixed polar angle model is when the azimuthal angle is sampled much faster than the excitation transfer rate. Three different static fixed polar angle distributions are shown in Figure 6, $\theta = 45°$, 60°, and 90° where θ is the angle between the transition dipoles of the chromophores and the surface normal. The ETISD process is fastest for $\theta = 90°$ and slowest for $\theta = 45°$, however, the change is not monotonic, as $\theta = 30°$ is about as fast as $\theta = 60°$ and $\theta = 0°$ is about as fast as $\theta = 90°$. These latter angles are not shown in the figure. For the static isotropic, dynamic isotropic (corresponding to $\kappa^2 = 2/3$ for all chromophores) and dynamic fixed polar

angle (corresponding to $\kappa^2 = 9/16$ for all chromophores) models, the ETISD occurs fastest in the dynamic isotropic and at a nearly equal but slower rate in the static isotropic and dynamic fixed polar angle models. The dynamic averages are either slower or faster than the static averages depending on the angular distribution used. Changing the angular distribution effectively changes the R_0's in the system by scaling the rate factors. This scaling changes the sensitivity of both ETISD and $G_s(t)$ to the underlying frequency distributions in different and nontrivial ways.

ETISD and $G_s(t)$ curves have also been calculated for three-dimensional systems. The results are illustrated in Figure 7. The trends are similar to the one- and two-dimensional cases. However, in three dimensions, the hard sphere and lattice models are more similar than in the 1D and 2D systems.

IV. APPROXIMATIONS TO THE ETISD PROBLEM

Baumann and Fayer have previously applied the Huber approximation[53] for ET in two- and three-dimensional systems.[16] The Huber approximation is useful when a simplified method is required to solve the ET problem. The key result from their work is that the natural logarithm of the self part of the Green's function (probability of initial excitation remaining on initially excited molecule) can be related to a configuration space integral over the ET probability kernel between the initially excited molecule and any other molecule in the system:

$$\ln G_s(t) = -\frac{\rho}{\lambda}\int_{r_0}^{+\infty} dr \times \int_\Omega d\Omega \left[1 - \exp\left(-\frac{3\lambda t R_0^6}{2\tau r^6}\kappa^2(\Omega)\right)\right] u(r)v(\Omega). \tag{10}$$

Here, ρ is the density, λ is a parameter which is 1 for donor-acceptor transfer and 2 for donor-donor transfer (the typical vibrational case), τ is the lifetime, $u(r)$ is the radial distribution function, and $v(\Omega)$ is the orientational probability density function. The above equation differs from Eq. (2.12) of Baumann and Fayer by the fact that the lower limit, which was 0 in the reference, is replaced by r_0, the exclusion radius. The exclusion radius is the distance below which the probability of finding a nearby molecule is 0.

Baumann and Fayer derive relations only in the case for $r_0 = 0$, but here we will generalize their results to work for any exclusion radius in a nearly analytical fashion. Following Baumann and Fayer, two substitutions are made: $y = \frac{\mu}{r^6}$, $\mu(\Omega; t) = \frac{3\lambda t R_0^6}{2\tau}\kappa^2(\Omega)$, resulting in the expression

$$\ln G_s(t) = -\frac{\rho}{\lambda}\int_0^{y(r=r_0)} dy \left(\frac{y}{\mu}\right)^{-\frac{7}{6}} \frac{1}{6\mu} \times \int_\Omega d\Omega[1 - \exp(-y(r, \Omega; t)]u(r)v(\Omega). \tag{11}$$

This is the most general result and can be further simplified in the cases of one, two and three dimensions if the radial distribution function is completely uniform except for the excluded volume effect. For dimension, $\Delta \in \{1, 2, 3\}$ and uniform radial distribution, $u(r) \in \{2, 2\pi r, 4\pi r^2\}$, the logarithm of the self part of the Green's function in the case where there is a non-negligible molecular volume may be expressed as

$$\ln G_s(t) = -c_\Delta \lambda^{\Delta/6-1}\left(\frac{3}{2}\right)^{\Delta/6}\left(\frac{t}{\tau}\right)^{\Delta/6}\int_\Omega d\Omega\kappa^{\Delta/3}(\Omega) \times \left[y_0(\Omega)^{-\Delta/6}(e^{-y_0(\Omega)} - 1) + \gamma\left(1 - \frac{\Delta}{6}, y_0(\Omega)\right)\right], \tag{12}$$

where $\gamma(\cdot,\cdot)$ is the lower incomplete Gamma function, and $y_0(\Omega) = \frac{1}{r_0^6}\frac{3\lambda t R_0^6}{2\tau}\kappa^2(\Omega)$ is the value of the dimensionless parameter y when r is at the exclusion radius (r_0) lower bound and the chromophores have a relative orientation of Ω in angular space. c_Δ is the reduced concentration which is equal to the density multiplied by the Förster volume, i.e., $c_\Delta = \rho V_\Delta$, where V_Δ is $2R_0$ for the one-dimensional case, $\pi {R_0}^2$ for the two-dimensional case, and $(4/3)\pi {R_0}^3$ for the three-dimensional case.[16]

In the isotropic dynamic limit, the configuration space integral disappears, $\kappa^2 = 2/3$, and the expression is replaced by

$$\ln G_s(t) = -c_\Delta \lambda^{\Delta/6-1}\left(\frac{t}{\tau}\right)^{\Delta/6} \times \left[y_{0,dyn}^{-\Delta/6}(e^{-y_{0,dyn}} - 1) + \gamma\left(1 - \frac{\Delta}{6}, y_{0,dyn}\right)\right], \tag{13}$$

where $y_{0,dyn} = \frac{1}{r_0^6}\frac{\lambda t R_0^6}{\tau}$.

Performing the angular average over the relative orientation of the chromophores is nontrivial and in the isotropic static case depends on four polar angles regardless of the dimension.[16] For the case of the fixed polar angle model (see the Appendix), the orientational average depends on only the two azimuthal angles with respect to the separation vector.

The Huber approximation is a two-particle model (in that the initial excitation is coupled outward to all nearby acceptors, but the acceptors are not inter-coupled) plus a first-order cumulant expansion truncation.[16,53] However, for a three-dimensional random distribution of molecules, $G_s(t)$ calculated with the Huber approximation and with a diagrammatic method involving an infinite number of particles and pathways[11] showed essentially perfect agreement.[6,54] This model is easily modified to encompass inhomogeneous lines. Instead of the initial excitation being coupled to an acceptor density, the initial excitation is coupled to many unconnected acceptor densities each with a different acceptor frequency. For each acceptor density the ET problem is solved independently, and then averages over all possible acceptor frequencies and initial excitation frequencies are performed. Mathematically, Eq. (12) is first exponentiated so that for each possible R_0 a $G_s(t)$ curve is generated. These $G_s(t)$ are then used to calculate the FFCF according to Eq. (5) (where the

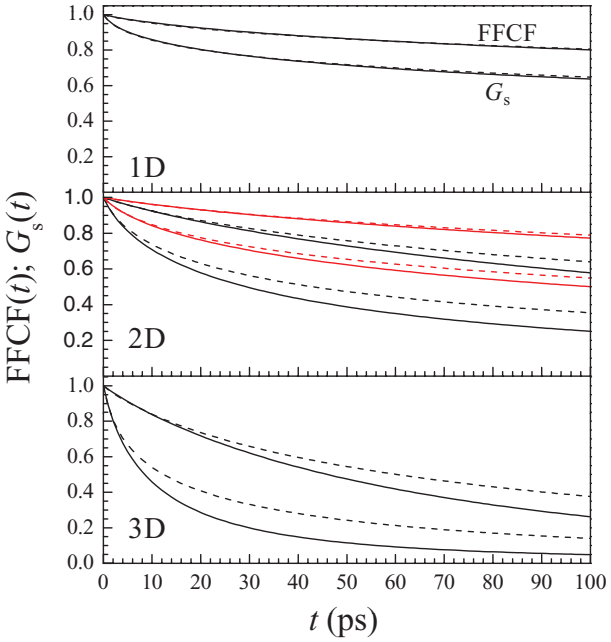

FIG. 8. (1D) 1D Huber approximation (dashed curves) and full Monte Carlo approach (solid curves). The top set of curves in the figure are normalized FFCFs with the homogeneous component omitted, and the lower set of curves the $G_s(t)$ curves. (2D) Same as 1D but for the two-dimensional system. Red curves are simulations at half the density of the black curves (1×10^{14} cm^{-2} vs 2×10^{14} cm^{-2}). (3D) Same as 1D but for the three-dimensional system.

two-particle Green's functions are replaced with the Huber Green's functions).

Figure 8 compares the Huber approximate solutions to the ETISD (FFCF) and ET ($G_s(t)$) problems to the Monte Carlo results for the random distribution with excluded volume model. The static isotropic angular distribution is used. In these calculations, the vibrational lifetime is 10 ps. The calculations go out to 100 ps. In a typical experiment, measurements can be made out to 2 to 4 vibrational lifetimes. $G_s(t)$ is only the decay of the probability of finding the excitation on the initially excited molecule. The decay of the probability of being on any molecule caused by the lifetime is a multiplicative exponential factor. The reduced Förster concentrations cannot be specified since they are based on the assumption of homogeneous lines and a single value of R_0. Here because the lines are inhomogeneously broadened and R_0 depends on the overlap of the homogenous lines, there is not a single R_0 or reduced concentration. The concentrations are very high. If the lines were homogeneously broadened, the 1D, 2D, and 3D reduced concentrations would be 1.5, 1.8, and 1.9. For the 2D case, a concentration of half this 2D value is also considered. The slower decaying pairs of curves are the FFCFs and the faster decaying pairs of curves are the $G_s(t)$s. The solid lines are from the full Monte Carlo solution to the ET problem and the dashed lines were calculated with the Huber approximation.

In Figure 8, the 1D Huber approximation to the normalized FFCF with the homogeneous contribution omitted and $G_s(t)$ are virtually identical to the Monte Carlo simulations for the entire simulation time. For the 2D case, the lower concentration curves (red, 1×10^{14} cm^{-2}) are very close. The FFCF Monte Carlo and Huber approximation calculations are virtually identical to 4 or 5 lifetimes, which is generally longer than experiments can be conducted. At the higher concentration in 2D (black curves, 2×10^{14} cm^{-2}), $G_s(t)$ has some error after about one lifetime, but the calculation of the FFCF is still very good out to about 3 lifetimes.

The agreement between the Huber approximation and the Monte Carlo simulations is much worse at the high concentration used in the calculations, although it improves rapidly as the concentration is reduced. The FFCF is quite good out to about two lifetimes. To get a feel for the error, the curves were fit to multi-exponentials. The FFCFs fit essentially perfectly with a bi-exponential, while the $G_s(t)$ curves require tri-exponentials to get an excellent fit. The fits to the FFCFs yield time constants of 25.3 ps and 335 ps (Huber) compared to 27.1 ps and 237 ps (Monte Carlo). The fits to $G_s(t)$ yield time constants of 3.6 ps, 20.7 ps, and 208 ps (Huber) compared to 3.9 ps, 20.8 ps, and 139 ps (Monte Carlo). For both the FFCF and $G_s(t)$, the agreement is very good for the short time components, but there is an error of ~30% on the long time components.

V. ETISD COUPLED TO STOCHASTICALLY FLUCTUATING FREQUENCIES (STRUCTURAL SPECTRAL DIFFUSION)

Excitation transfer is only one of the two mechanisms that can produce spectral diffusion. The other is SSD caused by microscopic changes in the inhomogeneous environments which molecules experience. For systems in which the vibrational chromophores are in high concentration, structural fluctuations occur simultaneously with the excitation transfer process. The goal of most nonlinear spectroscopic experiments in which the frequency-frequency correlation function is measured is to extract the SSD correlation function and not the ETISD correlation function. However, in order to extract the SSD correlation function it is necessary to have a firm understanding of the ETISD process. In the following, calculations and methods are presented that include both ETISD and SSD, and it is possible to extract the structural spectral diffusion. First a phenomenological model for SSD is introduced and then it is combined with ETISD.

A. Treating structural spectral diffusion

Structural spectral diffusion is associated with stochastic fluctuations affecting the underlying micro-states responsible for inhomogeneous broadening of absorption lines. Spectral diffusion processes are noise processes that are characterized by statistical autocorrelation functions. These statistical autocorrelation functions (time correlation functions), are typically measured using time-resolved spectroscopic techniques such as hole-burning[55] and 2D IR spectroscopy.[56] To simulate total spectral diffusion measured by one of these experiments, a phenomenological model of structural spectral diffusion must be developed that can be coupled to the ETISD problem.

Structural spectral diffusion can be modeled as a Langevin process.[57] The damping term of the Langevin

process ensures that the absorption frequency returns to line center and the random force results in fluctuations. This is essentially a filtered noise process with an exponential autocorrelation. The process is described by the following assumptions:

$$\frac{d\,(\delta\omega(t))}{dt} = -\gamma\delta\omega(t) + F(t), \tag{14}$$

$$\langle F(t)\rangle = 0;\ \langle F(t)F(t')\rangle = F_0\delta(t-t');\ \langle\delta\omega(t)F(t')\rangle = 0, \tag{15}$$

where $F(t)$ is a white Gaussian noise process with power spectral density F_0 and γ is the relaxation rate. The above assumptions state that the center frequency of a chosen oscillator evolves according to a Hookean differential equation that is noise driven, where the noise is uncorrelated with the frequency state variable and is a Gaussian random variable. The frequency process given by the above equation is a Gaussian random process and all moments (time correlation functions in the continuous time case) are related to the mean and covariance via the standard Gaussian relationships for moments. The Green's function solution to the differential equation is

$$\delta\omega(t) = e^{-\gamma t}\delta\omega(0) + \int_0^t F(\tau)e^{-\gamma(t-\tau)}d\tau. \tag{16}$$

To ensure strict-sense stationarity of the stochastic process it may be shown that $F_0 = 2\gamma\langle\delta\omega(0)^2\rangle$, where $\langle\delta\omega(0)^2\rangle$ is the variance of the frequency and defines the inhomogeneous linewidth in the absorption line being modeled. By substitution of

$$\delta\omega(s) = e^{-\gamma s}\delta\omega(0) + \int_0^s F(\tau)e^{-\gamma(s-\tau)}d\tau$$

into

$$\delta\omega(t) = e^{-\gamma t}\delta\omega(0) + \int_0^t F(\tau)e^{-\gamma(t-\tau)}d\tau$$

for times $s < t$, it is possible to show that $\delta\omega(t) = e^{-\gamma(t-s)}[\delta\omega(s)] + \int_s^t F(\tau)e^{-\gamma(t-\tau)}d\tau$. This relation implies that it is possible to increment the Langevin process by sampling from the following stochastic process:

$$\omega(t) = e^{-\gamma(t-s)}[\delta\omega(s)] + \varepsilon(t-s), \tag{17}$$

$$\varepsilon(t-s) \sim N(0, \langle\delta\omega(0)^2\rangle(1-e^{-2\gamma(t-s)})). \tag{18}$$

This procedure permits discrete time propagation of the stochastic process describing SSD on a continuous frequency grid with any time step. The continuous frequency distribution generated by the error term above can also be discretized onto a frequency grid for ease of simulation. In experiments that measure SSD, a mutli-exponential form of the FFCF is usually used in the data analysis.[58,59] The treatment given above yields a single exponential FFCF for the SSD. For multi-exponential FFCFs, multiple independent SSD processes can be simulated and their outputs simply added.

Figure 9 illustrates a sample simulation by the above method for an inhomogeneous width of 16 cm^{-1} and a SSD correlation time of 75 ps. Panel (a) shows a random trajectory

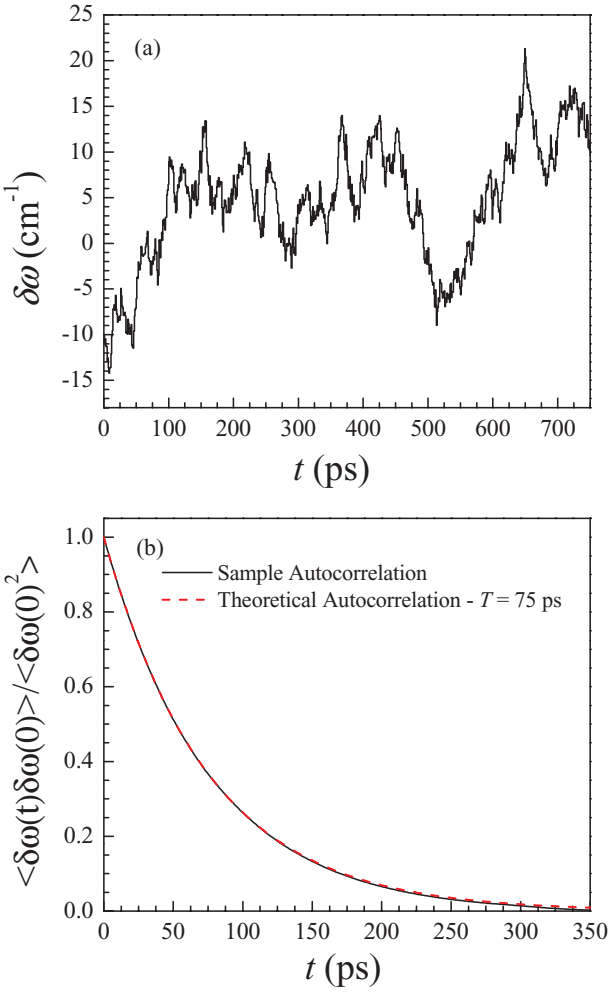

FIG. 9. (a) Example of a small piece of a simulated discrete time spectral diffusion noise process for a time constant of 75 ps and standard deviation of 16 cm^{-1}. (b) Theoretical normalized autocorrelation (red dashed curve) and normalized sample autocorrelation (solid black curve) from the noise process shown in panel (a).

of frequencies. Note that panel (a) is just a short snapshot of the total simulation. Panel (b) shows the numerically calculated normalized autocorrelation function (black curve) from the full trajectory. The red dashed line is the theoretical normalized autocorrelation (exponential decay of 75 ps). Clearly the two curves are essentially identical. The agreement demonstrates the accuracy of the simulation method. One caveat is that the simulated variance (45.75 cm^{-2}) is slightly lower than the theoretical variance (46.16 cm^{-2}) due to the effect of discretizing the frequency distribution. However, this discretization effect does not impact the simulated correlation time which is the most important feature of the model.

B. Multiplicative approximation to the coupled stochastic-dynamic system

Using the idea of propagating the SSD noise process by using a deterministic component plus a noise term, it is possible to build a multiplicative approximation to the FFCF of the coupled stochastic-dynamic system for coupled ET/SSD. The assumptions in this approximation are that there is a single

excitation and that there will be a sequential propagation of ET and SSD. First, ET will occur for a short time t, and then SSD will occur for a short time τ. Clearly, in the limit of small time steps this procedure will generate the correct dynamics.

To begin working with this approximation first we write down the FFCF in terms of iterated conditional expectation values:

$$\langle \delta\omega(t)\delta\omega(0)\rangle_{\mathrm{ET}(t)} = \mathrm{E}_{\delta\omega(0)}\mathrm{E}_{\delta\omega(t)|\delta\omega(0)}\left[\delta\omega(t)\omega(0)\,|\,\delta\omega(0)\right], \tag{19}$$

$$\langle \delta\omega(t+\tau)\delta\omega(0)\rangle_{\mathrm{ET}(t)+\mathrm{SSD}(\tau)} = \mathrm{E}_{\delta\omega(0)}\mathrm{E}_{\delta\omega(t+\tau)|\delta\omega(0)}\left[\delta\omega(t+\tau)\omega(0)|\delta\omega(0)\right]. \tag{20}$$

$\delta\omega(t)|\delta\omega(0)$ is determined by the ET process and is distributed as $P(\delta\omega(t)|\omega(0))$, which is $\mathbf{p}(t)$ from Eq. (8). $P(\delta\omega(t)|\omega(0))$ is the probability distribution given by the ET dynamic after a time t. Equation (19) is the short time propagation of the excitation transfer dynamic process. Equation (20) is the sequential propagation of the short time ET process followed by the short time SSD process. Expanding the probability law of the sequential ET/SSD process within Eq. (20) we achieve

$$\langle \delta\omega(t+\tau)\delta\omega(0)\rangle_{\mathrm{ET}(t)+\mathrm{SSD}(\tau)} = \mathrm{E}_{\delta\omega(0)}\mathrm{E}_{\delta\omega(t)|\delta\omega(0)}\mathrm{E}_{\varepsilon(\tau)}[(e^{-\gamma\tau}\delta\omega(t)+\varepsilon(\tau))\omega(0)\,|\,\delta\omega(0)], \tag{21}$$

where the SSD process has been propagated using the deterministic exponential multiplication and the noise term $\varepsilon(\tau)$ which is given by Eq. (18). We take apart the internal sum by linearity of expectation,

$$\langle \delta\omega(t+\tau)\delta\omega(0)\rangle_{\mathrm{ET}(t)+\mathrm{SSD}(\tau)} = e^{-\gamma\tau}\mathrm{E}_{\delta\omega(0)}\mathrm{E}_{\delta\omega(t)|\delta\omega(0)}\mathrm{E}_{\varepsilon(\tau)}\left[\delta\omega(t)\omega(0)\,|\,\delta\omega(0)\right] + \mathrm{E}_{\delta\omega(0)}\mathrm{E}_{\delta\omega(t)|\delta\omega(0)}\mathrm{E}_{\varepsilon(\tau)}\left[\varepsilon(\tau)\omega(0)\,|\,\delta\omega(0)\right]. \tag{22}$$

Clearly, the second term is zero since the error term in the SSD propagator has zero mean. The first term, referring to Eq. (19) is equal to

$$\langle \delta\omega(t+\tau)\delta\omega(0)\rangle_{\mathrm{ET}(t)+\mathrm{SSD}(\tau)} = e^{-\gamma\tau}\,\langle \delta\omega(t)\delta\omega(0)\rangle_{\mathrm{ET}(t)}, \tag{23}$$

which shows that within a short time approximation the coupled ET/SSD system behaves as the ET only FFCF multiplied by the normalized SSD FFCF. This motivates the approximation that the combined ET/SSD FFCF will be equal to that of the SSD FFCF multiplied by the ETISD only FFCF. Here we are considering a SSD FFCF that is a single exponential. As mentioned above, the SSD FFCF can have more terms than a single exponential. The time constant for the full FFCF will end up being different from the underlying SSD time constant as will be shown empirically for a number of systems in Sec. V C.

This approximation is not true at all times due to the fact that the SSD process intrinsically changes the statistical-dynamical law of ET, i.e., the $P_{\delta\omega(t)|\delta\omega(0)}$ is changed at later times in the propagation process. The SSD process, in fact, speeds up the ET dynamics because it pulls initially distant frequencies towards the center of the line due to the exponential damping term of the SSD process. This means that molecules that initially undergo slow excitation transfer will on average undergo faster excitation transfer at later times. This phenomenon is observed in calculations below.

C. Solving the coupled stochastic-dynamic system

Solving for the dynamics in the case of ETISD and SSD requires coupling the ET dynamic system with the stochastic fluctuations of SSD. Perhaps the most straightforward way to solve this problem on a discrete time grid of size N is to recursively build the N-dimensional probability distribution of frequencies that obey the SSD law. Unfortunately, this method results in a need to keep track of m^N probabilities and frequency vectors where m is the number of elements in the frequency grid upon which the SSD and ETISD problems are solved. This problem is clearly computationally impossible as N increases, and therefore is more efficiently solved by Monte-Carlo averaging over frequency trajectories sampled from the stochastic SSD system.

The method of coupling the two dynamic systems is to co-propagate their state variables. For example, in a single time step, first new frequencies are drawn from the stochastic SSD process and then, using populations on the vibrational chromophores from the previous time step, new populations are calculated according to the dynamic law governing ET. This method will first be developed in an ensemble of particle pairs case, extended to the N-particle case, and finally approximations to allow faster calculation of ETISD in the presence of SSD will be presented.

1. The ensemble of particle pairs case

For the ensemble of pairs of vibrational chromophores with no interactions between pairs, the discrete time-frequency SSD coupled ETISD problem can be solved exactly given a random discrete time trajectory along the given frequency grid. If the probability of the excitation lying on the initially excited molecule at a time t is denoted by $E_0(t)$, then $E_0(t+\tau)$ is given by

$$E_0(t+\tau) = \frac{1}{2}\left(1 + e^{-2k(\omega_0(t),\omega_1(t))\tau}(2E_0(t)-1)\right), \tag{24}$$

where $k(\omega_0(t),\omega_1(t))$ is the Förster transfer rate at the time t due to the current values of the stochastic time-dependent frequencies ω_0 and ω_1. In the ensemble of particle pairs case, only a single variable (E_0) must be carried between time steps due to the law of total probability, in the N-dimensional case at least N−1 probabilities must be accounted for at every time step. As it will be useful in developing further approximations to this problem, we also develop a graphical method for propagating the ET system when SSD is occurring simultaneously. The process, which is equivalent to the algebraic method of Eq. (24), is illustrated in Figure 10. At the start of a new time step from t to $t+\tau$, the remaining initially excited population E_0 is found on the new dynamic system curve for the new frequencies drawn from the stochastic process. The remaining initially excited population

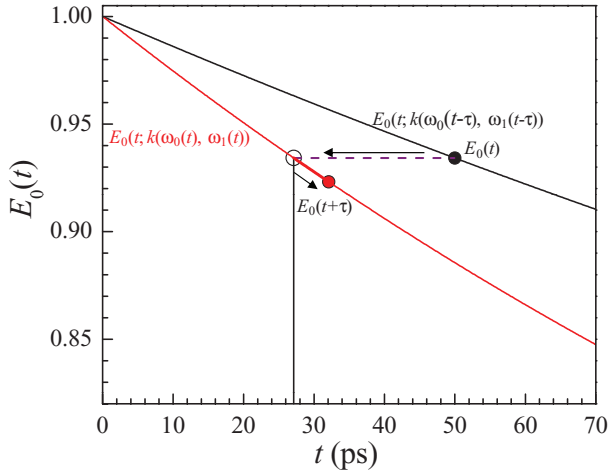

FIG. 10. Graphical procedure for coupled dynamic/stochastic system propagation. At the start of a new time step from t to $t + \tau$ the remaining initially excited population, E_0, is found on the new dynamic system curve for the new frequencies drawn from the stochastic process. The remaining initially excited population is then propagated down the new dynamic system curve for τ. This method is equivalent to the algebraic propagation in Eq. (19). This method may be used for propagation of the Huber approximation coupled to a stochastic spectral diffusion process, or any other method for estimating $G_s(t)$ as a function of frequency pairs.

is then propagated down the new dynamic system curve for τ. For each trajectory and time step the contribution of a particular trajectory to the Monte Carlo averaged FFCF is calculated by Eq. (8).

For the standard two-particle parameters outlined in the Appendix, we have solved the SSD coupled ETISD problem for various SSD rates. The results (solid black curves) are the total normalized FFCFs with the homogeneous component omitted shown in Figure 11(a). The dashed black curve, which is the top curve in each panel, is the FFCF for ETISD in the absence of SSD. The coupled SSD and ETISD problem was also solved for the case of a separation distance of 5 Å, for which ET and, therefore, the ETISD is faster (Figure 11(b)). The SSD ranges from slow, 800 ps, which is comparable to the ETISD, to fast, 25 ps, which is much faster than the ETISD.

Figure 11 also illustrates the multiplicative approximation to the coupled ETISD and SSD problem. The red dashed curves are the result of fitting the properly calculated total spectral diffusion, which has contributions from ETISD influenced by SSD and SSD, to the form of an exponential decay multiplied by the ETISD with no SSD (dashed black curves) as suggested by the approximation discussed above. The SSD exponential time constant obtained from the fit using the multiplicative approximation is not equal to the true time constant of the SSD stochastic process. However, the important result is that the SSD time constants from the multiplicative approximation are close to the true SSD time constants. Figure 12 illustrates the true SSD process time constants plotted against the multiplicative approximation SSD fit time constants for both $d = 8.0$ Å and $d = 5.0$ Å. The dashed line is at 45°, which would be the result if the multiplicative approximation was perfect. It is a guide to the eye to make it easier to see the error in the multiplicative approximation. For the

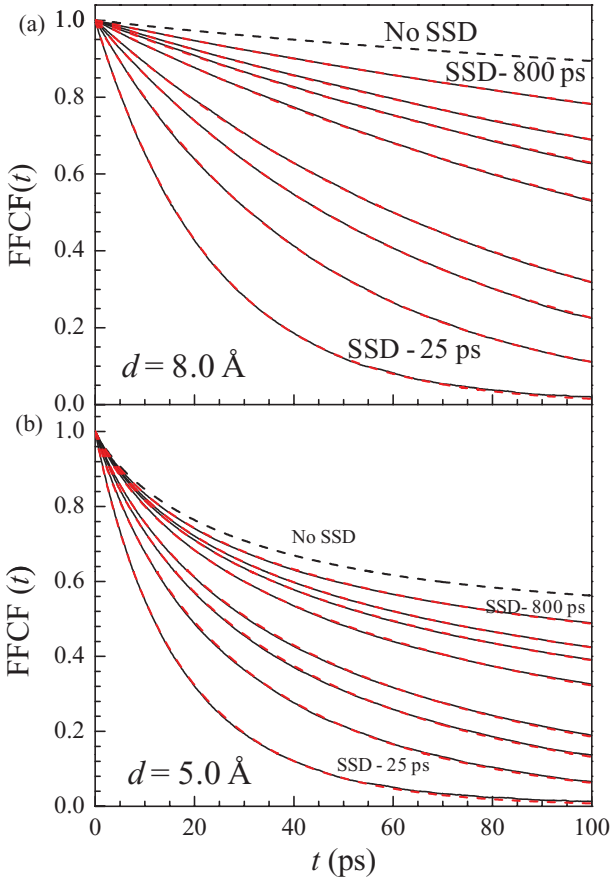

FIG. 11. Normalized FFCFs with the homogeneous component omitted for the ensemble of particle pairs ET models with SSD processes co-propagated. The FFCFs from the coupled ET/SSD process (solid black) are calculated for SSD time constants of 25 ps, 50 ps, 75 ps, 100 ps, 200 ps, 300 ps, 400 ps, and 800 ps. The dashed black curve is the FFCF due to ETISD without any accompanying SSD process. The red dashed curves are fits to the coupled ET/SSD FFCFs by assuming the profile is created by an exponential decay multiplied by the non-SSD coupled ETISD curve. Labels lie above their respective curves. (a) Pair separation distance, $d = 8$ Å. (b) Pair separation distance, $d = 5$ Å.

$d = 5.0$ Å the actual time constant is 1.12 times the time constant obtained from the multiplicative approximation, and for the $d = 8.0$ Å the actual time constant is 1.058 times the approximate time constant. With $d = 5.0$ Å, excitation transfer is very fast. Even in this case, the multiplicative approximation does not produce severe error in the determination of SSD.

The fact that the multiplicative approximation (red and blue lines in Figure 12(a)) yields SSD that is faster than the input process is caused by the fact that SSD speeds up ET. Therefore, the ETISD contribution to the total FFCF is faster than the FFCF with no SSD that is used in the approximation. The enhancement in the FFCF decay is caused by the enhancement of ETISD by coupling to SSD, as the SSD process is not modified by excitation transfer. The SSD process creates a stochastic grid of frequencies upon which the ETISD problem is solved. The stochastic nature of the frequency grid changes the nature of the ET process. Figure 12(b) shows that the ensemble averaged $G_s(t)$ curves decay faster when SSD is included in the model, demonstrating the predicted result of coupling between SSD and ETISD.

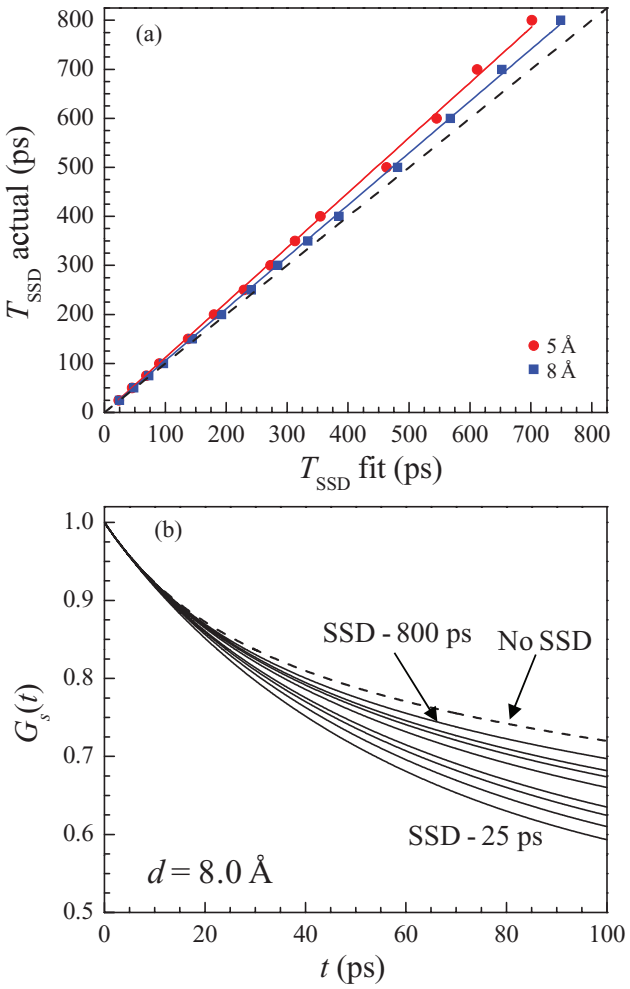

FIG. 12. (a) Actual time constant of SSD process versus the one determined by assuming SSD can be approximated by an exponential decay multiplied by the ETISD curve calculated without the influence of SSD. The system is the ensemble of particle pairs with the separations $d = 8$ Å (blue squares) and $d = 5$ Å (red diamonds). Solid lines are linear fits ($R^2 > 0.999$). The dashed line is an aid to the eye that would occur if the approximation gave the correct result. The true time constant is always longer than the fit time constant, demonstrating that the ET/SSD coupling results in faster ETISD than would occur without the two processes being coupled. The faster the ET occurs, the faster the fit time is relative to the actual time. (b) Enhancement of the underlying ET process by the inclusion of SSD is observed through the self part of the Green's function for the $d = 8$ Å case. $G_s(t)$ curves are shown when SSD is excluded (dashed curve) and for the ET coupled to SSD with time constants between 25 ps and 800 ps (solid curves; same time constants as in Figure 11). $G_s(t)$ decays faster as the SSD process becomes faster.

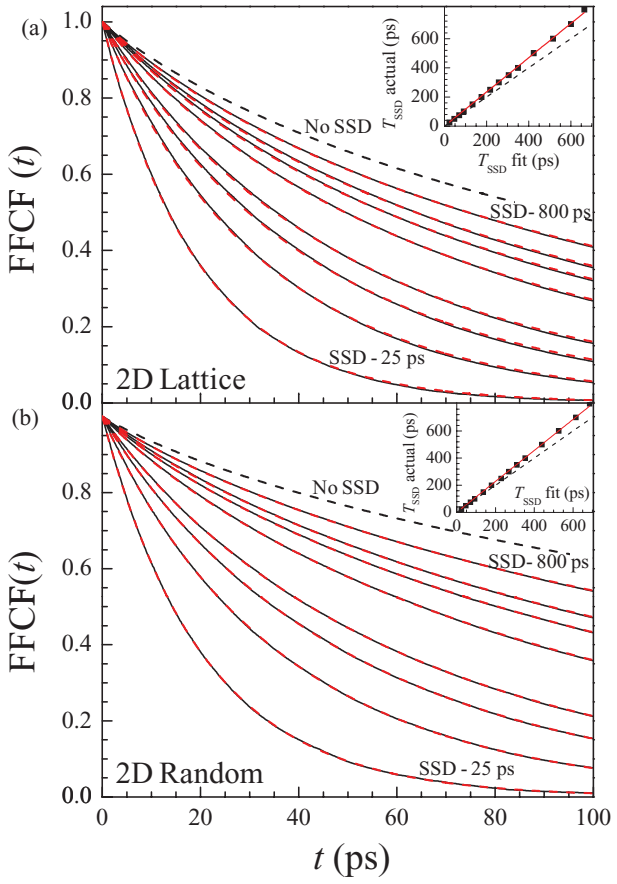

FIG. 13. Results of full coupled ET/SSD calculation for two 2D geometries. (a) Normalized FFCFs with the homogeneous component omitted for the 2D HCP lattice system (with fixed polar angle model with $\theta = 45°$) for 25-800 ps SSD time constants (same as in Figure 11). Dashed curve is ETISD profile without coupling to SSD. Black solid curves are the FFCFs from the full Monte Carlo solutions to the coupled ET/SSD problem. Red dashed curves are the result of assuming that FFCF can be approximated as an exponential decay multiplied by the ETISD curve calculated with no SSD. Labels lie above their respective curves. (a, inset) Comparison of the multiplicative approximation time constants to the simulated SSD time constants (squares). Red line is a linear fit with a slope of 1.17. The dashed line is an aid to the eye that would occur if the approximation gave the correct result. (b) Normalized FFCFs with the homogeneous component omitted for the 2D random with excluded volume system (with fixed polar angle model with $\theta = 45°$) for 25-800 ps SSD time constants. Curves are as in Panel (a). Labels lie above their respective curves. (b, inset) Comparison of the multiplicative approximation time constant to the simulated SSD time constant (squares). Red line is a linear fit with a slope of 1.14. The dashed line is an aid to the eye that would occur if the approximation gave the correct result.

2. N-particle case

The general N-particle case corresponds to any system – 1D, 2D, 3D, periodic, or non-periodic. Before describing results for a specific system, the general methodology will be revisited.

To solve the N-particle system, at each time step the instantaneous frequencies drawn from the SSD process are used to calculate the matrix propagator given by Eq. (7) for a simulation time step of τ. This propagator is used to update the frequency probabilities for the initial excitation as it is tracked across the manifold of acceptors. The new probability vector is passed to the next iteration and a new propagator is calculated using the new frequencies given by the SSD process progression.

As all N-particle systems are essentially the same problem, we show only a calculation of the SSD coupled ETISD problem for a two-dimensional hexagonal lattice model and the random distribution with excluded volume model using the parameters from the Appendix. The angular model is a fixed polar angle model with a 45° angle with respect to surface normal. Figure 13(a) shows the results for the 2D hexagonal lattice case. The dashed black curve is the normalized FFCF with the homogeneous component omitted with no SSD. The solid black curves are the FFCFs for the systems with SSD time constants ranging from 25 to 800 ps. Clearly, as the SSD rate increases, the FFCF decays more rapidly. The

dashed red curves are the result of assuming that the FFCF can be approximated by an exponential decay multiplied by the ETISD FFCF with SSD omitted. A single exponential is used due to the underlying single exponential SSD process. This approximation agrees reasonably well with the full simulations. The inset of Figure 13(a) shows the relationship between the time SSD constants used in the multiplicative approximation to the FFCF and the underlying SSD time constants. A smaller time constant in the fit is indicative of enhancement of the underlying ET process as discussed above in the ensemble of particle pairs case. In this case the true underlying time constant is 1.17 times the fit constant. Figure 13(b) shows similar results for the 2D random distribution with excluded volume model. Again, the normalized FFCF with homogeneous component omitted is shown for the case of no SSD (dashed curve) and SSD time constants between 25 ps and 800 ps (solid black curves). The red dashed curves show the approximation that the FFCF is equal to an exponential decay multiplied by the ETISD FFCF with SSD omitted. Again this approximation agrees well with the FFCFs from the full simulation. The inset in Figure 13(b) shows the agreement between the fit time constant and the true time constant input into the simulation. For this system the true underlying time constant is 1.14 times the fit time constant. There is a common trend in the enhancement factors across all systems simulated, both pairs of particles and N particles. The faster ETISD occurs without SSD, the faster the apparent exponential decay time constant is relative to the underlying SSD process time constant due to the enhancement effect of SSD on ET.

The multiplicative approximation (that the measured FFCF is equal to the SSD FFCF multiplied by the ETISD only FFCF) allows for the estimation of SSD process rates for systems undergoing simultaneous ETISD and SSD even when SSD has not been included in the calculation of ETISD. Therefore, it is possible for the experimentalist to assess the rate of SSD in the system once a model for ET has been chosen. The error in using this approximation has been shown to be on the order of 5%–20% for systems undergoing ET at the rates illustrated in this paper.

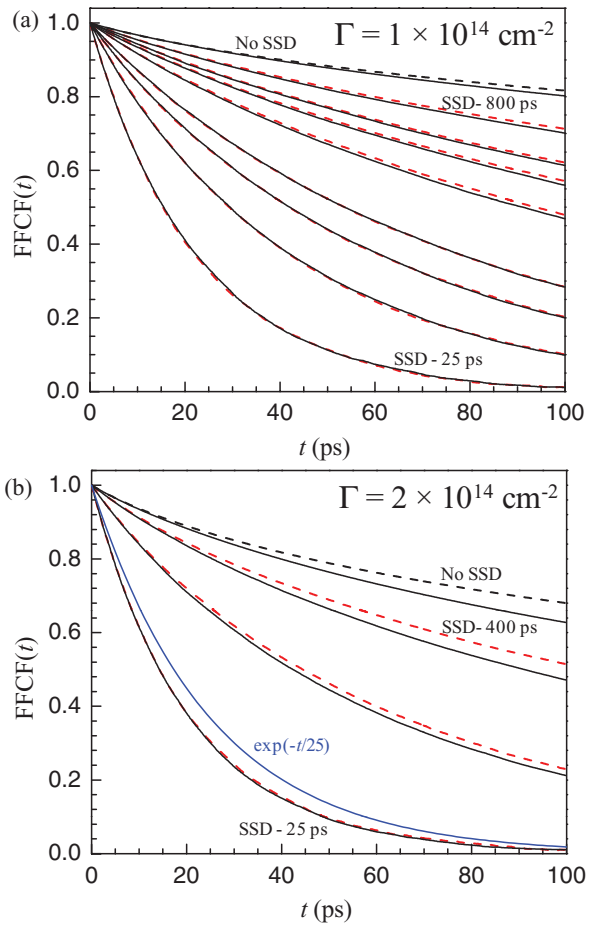

FIG. 14. (a) Comparison of normalized FFCFs with the homogeneous component omitted for combined ET/SSD models from a 2D random spatial distribution (with fixed polar angle model, $\theta = 45°$) using the full Monte Carlo method (black curves) and the Huber method (dashed red curves) for SSD time constants from 25 ps to 800 ps (same as in Figure 11). The slowest decaying curves (both dashed and solid) have no SSD process. Surface density (Γ) is set to 1×10^{14} cm^{-2}. Labels lie above their respective curves. (b) Same quantities except for a surface density (Γ) of 2×10^{14} cm^{-2} and SSD time constants of 25 ps, 100 ps, and 400 ps. The blue curve shows an exponential decay of 25 ps, illustrating that even when SSD is fast compared to ETISD calculated with no SSD the use of an ET model significantly alters the curve shape. The slowest decaying curves (both dashed and solid) have no SSD process. Except for the bottom most curve, labels lie above their respective curves.

3. Coupled ETISD and SSD within the Huber approximation

The Huber approximation can be used to solve the coupled ET/SSD problem using the graphical propagation method illustrated in Figure 10. First, two frequency vectors are independently drawn from the SSD noise process. Using the $G_s(t)$ curves from the Huber calculation for each frequency, the ET process is solved. Specifically, the intersection between the remaining probability of excitation on the initially excited molecule is denoted as $E_0(t)$ ($E_0(0) = 1$), with the $G_s^{\{\omega_1,\omega_2\}}(t)$ curve for the two SSD drawn frequencies ω_1, ω_2 at the time t. The initial excitation is then updated to the new value $E_0(t+\tau) = G_s^{\{\omega_1,\omega_2\}}(t+\tau)$ where τ is the simulation time step and the process is repeated. The FFCF is calculated in the same manner as for the ensemble of particle pairs case.

Figure 14(a) illustrates the agreement between the normalized FFCFs with the homogeneous component omitted for the coupled ETISD/SSD problem solved within the Huber approximation and the full Monte-Carlo solution for the half-density (1×10^{14} cm^{-2}) 2D system. The lines are plotted in pairs of solid (full Monte Carlo calculation) and dashed (Huber approximation) curves. The top pair (dashed black curve; solid black curve) are for the case of no SSD (these curves are the same as the red curves shown in Figure 8 - 2D). The next eight pairs of curves (red dashed curves; black solid curves) correspond to simulations with SSD time constants of 800–25 ps. The Huber approximation in this low density case agrees excellently with the full Monte Carlo calculation. Interestingly, as the SSD rate increases the Huber approximation improves in agreement which is best seen in the deviation of the dashed and solid curves at 100 ps. The SSD

dependent agreement is due to the fact that as the ETISD becomes less of a factor in determining the overall FFCF, the accuracy of the ETISD solution is less important. Figure 14(b) shows the comparison between the higher density (2×10^{14} cm^{-2}) SSD/Huber approximation and the full Monte-Carlo solution. As in panel (a), the top pair of curve (dashed – Huber; solid – full Monte Carlo) is for the case of no SSD (these are the black curves from Figure 8 - 2D). The next three pairs of curves (red dashed – Huber; black solid – full Monte Carlo) are for the SSD time constants 400ps, 100ps, and 25 ps. The agreement of the Huber approximation in the case of no SSD is seen to be quite good up to about 30 ps, after which it rapidly degrades. This is discussed above and is due to the high concentration chosen for the simulations. The agreement however improves as the SSD rate is increased. At a time constant of 25 ps, the agreement is essentially quantitative. To illustrate that the SSD coupled Huber approximation with a fast time constant is still different from just assuming that ETISD is negligible (i.e., the FFCF is just the SSD component), an exponential decay of 25 ps is shown as well (blue curve). Even when SSD is fast relative to ETISD, including the ET process is important, as fitting the FFCF with a single exponential decay SSD only model results in a decay time of 21 ps, a 16% additional error. These results indicate that the SSD coupled Huber approximation is a valid approximation to the full Monte-Carlo simulation approach, and is essentially exact when SSD is much faster than ETISD without SSD. It is conducive to use this method when the Monte-Carlo method requires excessive computation and the radial distribution function of the system allows for easy calculation of the integral in Eq. (11).

VI. CONCLUDING REMARKS

The theory developed above to describe ETISD in the case of both static and stochastic fluctuating inhomogeneities is broadly useful throughout spectroscopy. In any dense system in which excitation transfer can occur, our theory can help elucidate the underlying spectral dynamics. Furthermore, other experimental observables often depend implicitly upon the excitation transfer process such as the orientational anisotropy. Observables can only be fully understood after accounting for the impact of ET, which depends on SSD. Since the ET is itself modified by any underlying SSD processes, a full understanding of the spectral dynamics is necessary to interpret any experiment in systems where the distance between chromophores approaches the Förster radius that would apply for homogeneously broadened lines. For measurements of SSD, even when the SSD is much faster than ETISD determined in the static limit, substantial errors are possible if ET is not accounted for. Fast SSD does not overwhelm ETISD calculated in static limit because SSD causes ETISD to become faster than the static limit. As the rate of SSD increases, so does the rate of ETISD. To properly account for ET, it is necessary to know the homogeneous linewidth and the SSD. Only in systems in which the homogeneous linewidth is close to the total linewidth the standard Förster method can be used because there is essentially no SSD.

Specifically, we have solved the "forward" problem; given a set of parameters that describe excitation transfer and structural spectral diffusion, the FFCF (or any other observable) may be calculated. To solve the "inverse" problem, that is, given the data, it is desired to determine the dynamical parameters, which is the problem faced by the experimentalist, one would simulate a combined ET/SSD system much like the above cases and vary the parameters of interest until agreement with the experiment is obtained. Specifically, we recommend the following protocol given that an experimentalist wishes to measure an observable which depends on excitation transfer. First, measure the parameters required to simulate the excitation transfer, which includes the transition dipole moment, the non-radiative lifetime (which combined with the transition dipole gives the quantum yield[60]), the homogeneous linewidth, and the inhomogeneous linewidth. If the system undergoes spectral diffusion, then the experimental spectral diffusion must be measured using 2D IR or another method. By simulating the coupled ET/SSD system and comparing the FFCF to the experimental FFCF, it is possible to extract the underlying SSD time constant(s). Only now is it correct to calculate another observable that depends on the excitation transfer. For example, suppose the observable of interest is the orientational anisotropy. Only after accounting for coupled ETISD and SSD is it possible to determine the amount of anisotropy decay due to excitation transfer. Excess anisotropy decay beyond the amount due to excitation transfer can be attributed to orientational relaxation.

The theory presented here also illustrates the broad utility of ultrafast nonlinear optical spectroscopy and specifically techniques such as two-dimensional infrared spectroscopy. Only such techniques can extract the underlying homogeneous and inhomogeneous linewidths of chromophores. These linewidths are necessary inputs into a microscopic model of the ET or ETISD process. Furthermore, techniques such as 2D IR can probe the spectral diffusion, another necessary input for calculating the ETISD process. Without such techniques it is impossible to take apart the underlying dynamics.

The Monte-Carlo based techniques developed here also have broad applications in the molecular simulation community. Instead of full quantum mechanical models, it is possible to build our dynamic system approach on top of classical MD. The structures upon which the ET dynamic system is solved can be sequential snapshots from a MD simulation. Excitation transfer can therefore be incorporated into MD models of spectroscopic line shapes quite easily. This extension of the methods discussed above into MD simulations will permit the study of systems where translational and rotational motions happen on the time scales of excitation transfer.

ACKNOWLEDGMENTS

We thank the Air Force Office of Scientific Research under Grant No. FA9550-12-1-0050 for support of this research. D.E.R. also thanks the Fannie and John Hertz Foundation,

the National Science Foundation, and the Stanford Graduate Fellowship programs for graduate fellowships.

APPENDIX: PARAMETERS USED FOR EXCITATION TRANSFER CALCULATIONS

To illustrate trends and the underlying physics of excitation transfer induced spectral diffusion, consistent model parameters were used across all simulations. The values used are representative of many molecular systems but do not correspond to a specific one.

The "chromophore" modeled has a vibrational resonance at 5 μm (2000 cm^{-1}) with an integrated absorption strength of 1.8×10^4 M^{-1} cm^{-2} (integration performed in wave numbers), in a medium of index of refraction 1.4 corresponding to a transition dipole moment of 0.34 D in a medium of index of refraction 1.4. The "measured" lifetime is 10 ps which is taken to be the non-radiative lifetime. Combining the non-radiative lifetime with the transition dipole moment it is calculated[60] that the quantum yield is 4.1×10^{-9}. The homogeneous (Lorentzian) linewidth, except where noted otherwise, is taken to be 2 cm^{-1}. The inhomogeneous (Gaussian) linewidth, except where noted otherwise, is taken to be 16 cm^{-1}. The full linewidth using these two linewidths is 17.093 cm^{-1}. The frequencies were gridded on a 0.5 cm^{-1} mesh and the grid was allowed to extend to 2.5 inhomogeneous half widths in either direction from the line center leaving a 0.32% chance of finding a center frequency outside of the simulated region.

For ensemble of pairs of particle systems, the two particles are taken to be 8 Å apart and κ^2 is taken to be in the dynamic limit and equal to 2/3.

For one-dimensional systems, a density of 1.43×10^7 molecules/cm is used, which corresponds to a lattice constant of 7 Å for the one-dimensional lattice. The hard sphere model simulation was run with a hard sphere radius of 2.62 Å and the exclusion radius in the random simulation was set to 5.0 Å. All simulations were performed in boxes of ~120 Å length. Angular models for the 1D system were statically averaged and isotropically distributed.

For the two-dimensional systems simulated, the density is assumed to be 2×10^{14} molecules/cm^2 except where otherwise noted. The molecular diameter (exclusion radius) is taken to be 6 Å for the random distribution with excluded volume model, except where otherwise noted. The hard sphere radius for the loosely packed hard sphere model was 2.92 Å. Prior to Sec. V, except where otherwise noted, the distribution of angles is static and isotropic. For the coupled SSD/ETISD calculations a fixed polar angle model is assumed. The polar angle, θ, of the transition dipole away from the surface normal is assumed to be 45°. The azimuthal angle that describes the orientation of the transition dipole in the surface plane has a uniform random distribution. For this fixed polar angle model, given the angles φ_d and φ_a denoting the azimuthal angles of the donor and acceptor chromophores away from the donor-acceptor separation vector, $\kappa(\varphi_1, \varphi_2, \theta) = \cos^2(\theta) + \sin^2(\theta)(\sin(\varphi_1)\sin(\varphi_2) - 2\cos(\varphi_1)\cos(\varphi_2))$. Simulations were run in 60 Å by 60 Å boxes.

For three-dimensional systems, the transition moments are isotropically distributed in either the dynamic or static limits and a single density is simulated 2.92×10^{21} molecules/cm^3. This corresponds to a 7 Å lattice constant in a simple cubic lattice. The hard sphere model for 3D systems was run with a hard sphere radius of 3.0 Å and the exclusion radius in random with excluded volume models was set to 6.0 Å. Random and hard sphere models were run in a cube with 30 Å sides.

For all simulations other than the ensemble of particle pairs simulations, periodic boundary conditions were enforced by the minimum image criterion. Hard sphere distributions were generated by filling a volume with fixed position hard spheres randomly until no more spheres could be added.

[1] T. W. J. Gadella, *FRET and FLIM Techniques* (Elsevier Science, Boston, 2009).
[2] D. L. Andrews and A. A. Demidov, *Resonance Energy Transfer* (Wiley, New York, 1999).
[3] P. Wu and L. Brand, Anal. Biochem. **218**, 1 (1994).
[4] T. Förster, Rad. Res. Suppl. **2**, 326 (1960).
[5] H. Morawetz, Science. **240**, 172 (1988).
[6] K. A. Peterson, M. B. Zimmt, S. Linse, R. P. Domingue, and M. D. Fayer, Macromolecules **20**, 168 (1987).
[7] A. D. Stein, K. A. Peterson, and M. D. Fayer, Chem. Phys. Lett. **161**, 16 (1989).
[8] M. D. Ediger, R. P. Domingue, and M. D. Fayer, J. Chem. Phys. **80**, 1246 (1984).
[9] A. D. Stein and M. D. Fayer, J. Chem. Phys. **97**, 2948 (1992).
[10] D. P. Millar, R. J. Robbins, and A. H. Zewail, J. Chem. Phys. **75**, 3649 (1981).
[11] C. R. Gochanour, H. C. Andersen, and M. D. Fayer, J. Chem. Phys. **70**, 4254 (1979).
[12] D. Rehm and K. B. Eisenthal, Chem. Phys. Lett. **9**, 387 (1971).
[13] K. B. Eisenthal, Chem. Phys. Lett. **6**, 155 (1970).
[14] R. F. Loring and M. D. Fayer, Chem. Phys. **70**, 139 (1982).
[15] P. Anfinrud, R. L. Crackel, and W. S. Struve, J. Phys. Chem. **88**, 5873 (1984).
[16] J. Baumann and M. D. Fayer, J. Chem. Phys. **85**, 4087 (1986).
[17] I. V. Gopich and A. Szabo, J. Phys. Chem. B **111**, 12925 (2007).
[18] R. P. Haugland, J. Yguerabide, and L. Stryer, Proc. Natl. Acad. Sci. U.S.A. **63**, 23 (1969).
[19] T. Ha, T. Enderle, D. S. Chemla, and S. Weiss, IEEE J. Sel. Top. Quantum Electron. **2**, 1115 (1996).
[20] L. Stryer and R. P. Haugland, Proc. Natl. Acad. Sci. U.S.A. **58**, 719 (1967).
[21] P. R. Selvin, Nat. Struct. Biol. **7**, 730 (2000).
[22] T. L. C. Jansen, B. M. Auer, M. Yang, and J. L. Skinner, J. Chem. Phys. **132**, 224503 (2010).
[23] M. Yang, F. Li, and J. L. Skinner, J. Chem. Phys. **135**, 164505 (2011).
[24] H. Bian, X. Wen, J. Li, H. Chen, S. Han, X. Sun, J. Song, W. Zhuang, and J. Zheng, Proc. Natl. Acad. Sci. U.S.A. **108**, 4737 (2011).
[25] H. T. Bian, H. L. Chen, J. B. Li, X. W. Wen, and J. R. Zheng, J. Phys. Chem. A **115**, 11657 (2011).
[26] N. E. Levinger, R. Costard, E. T. J. Nibbering, and T. Elsaesser, J. Phys. Chem. A **115**, 11952 (2011).
[27] D. E. Rosenfeld, Z. Gengeliczki, B. J. Smith, T. D. P. Stack, and M. D. Fayer, Science. **334**, 634 (2011).
[28] K. S. Schweizer and D. Chandler, J. Chem. Phys. **76**, 2296 (1982).
[29] J. D. Eaves, A. Tokmakoff, and P. L. Geissler, J. Phys. Chem. A **109**, 9424 (2005).
[30] K. W. Kwak, S. Park, and M. D. Fayer, Proc. Natl. Acad. Sci. U.S.A. **104**, 14221 (2007).
[31] M. C. Thielges and M. D. Fayer, "Protein dynamics studied with ultrafast two-dimensional infrared vibrational echo spectroscopy," Acc. Chem. Res. (in press).
[32] K. J. Gaffney, I. R. Piletic, and M. D. Fayer, J. Chem. Phys. **118**, 2270 (2003).
[33] S. Woutersen and H. J. Bakker, Nature (London) **402**, 507 (1999).

[34]S. Woutersen, U. Emmerichs, and H. J. Bakker, J. Chem. Phys. **107**, 1483 (1997).
[35]J. B. Asbury, T. Steinel, K. Kwak, S. A. Corcelli, C. P. Lawrence, J. L. Skinner, and M. D. Fayer, J. Chem. Phys. **121**, 12431 (2004).
[36]D. Kraemer, M. L. Cowan, A. Paarmann, N. Huse, E. T. J. Nibbering, T. Elsaesser, and R. J. D. Miller, Proc. Natl. Acad. Sci. U.S.A. **105**, 437 (2008).
[37]T. Forster, Ann. Phys. **2**, 55 (1948).
[38]J. Lakowicz, *Principles of Fluorescence Spectroscopy* (Kluwer Academic/Plenum, New York, 1999).
[39]K. Kwak, S. Park, I. J. Finkelstein, and M. D. Fayer, J. Chem. Phys. **127**, 124503 (2007).
[40]J. Bredenbeck, J. Helbing, R. Behrendt, C. Renner, L. Moroder, J. Wachtveitl, and P. Hamm, J. Phys. Chem. B **107**, 8654 (2003).
[41]A. S. Agabekyan, Opt Spektrosk. **29**, 37 (1970).
[42]A. S. Agabekyan, Opt Spektrosk. **30**, 247 (1971).
[43]E. N. Bodunov and V. A. Malyshev, Opt Spektrosk. **46**, 487 (1979).
[44]G. D. Scholes, X. J. Jordanides, and G. R. Fleming, J. Phys. Chem. B **105**, 1640 (2001).
[45]S. E. Bradforth, R. Jimenez, F. Vanmourik, R. Vangrondelle, and G. R. Fleming, J. Phys. Chem. **99**, 16179 (1995).
[46]G. D. Scholes and G. R. Fleming, J. Phys. Chem. B **104**, 1854 (2000).
[47]G. D. Scholes, Annu. Rev. Phys. Chem. **54**, 57 (2003).
[48]A. D. Stein, K. A. Peterson, and M. D. Fayer, J. Chem. Phys. **92**, 5622 (1990).
[49]S. Jang, J. Chem. Phys. **127**, 174710 (2007).
[50]J. Seogjoo, J. Younjoon, and R. J. Silbey, Chem. Phys. **275**, 319 (2002).
[51]S. Jang, Y.-C. Cheng, D. R. Reichman, and J. D. Eaves, J. Chem. Phys. **129**, 101104 (2008).
[52]K. Kwak, D. E. Rosenfeld, and M. D. Fayer, J. Chem. Phys. **128**, 204505 (2008).
[53]D. L. Huber, D. S. Hamilton, and B. Barnett, Phys. Rev. B **16**, 4642 (1977).
[54]K. A. Peterson and M. D. Fayer, J. Chem. Phys. **85**, 4702 (1986).
[55]S. Volker, Annu. Rev. Phys. Chem. **40**, 499 (1989).
[56]J. Zheng, K. Kwak, and M. D. Fayer, Acc. Chem. Res. **40**, 75 (2006).
[57]S. Chandrasekhar, Rev. Mod. Phys. **15**, 1 (1943).
[58]J. R. Schmidt, N. Sundlass, and J. L. Skinner, Chem. Phys. Lett. **378**, 559 (2003).
[59]J. K. Chung, M. C. Thielges, S. E. J. Bowman, K. L. Bren, and M. D. Fayer, J. Am. Chem. Soc. **133**, 6681 (2011).
[60]R. C. Hilborn, Am. J. Phys. **50**, 982 (1982).